



AD-A191 493

AFGL-TR-87-0264

4

DTIC FILE COPY

Regional Studies With Broadband Data

Thomas V. McEvilly
Lane R. Johnson

University of California
Geology and Geophysics
Berkeley, CA 94720

DTIC
ELECTE
FEB 16 1988
S D

29 August 1987

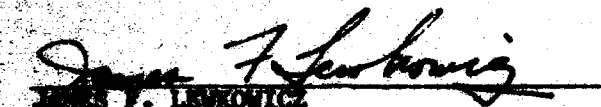
Final Report
13 February 1985 - 12 May 1987

APPROVED FOR PUBLIC RELEASE; DISTRIBUTION UNLIMITED

AIR FORCE GEOPHYSICS LABORATORY
AIR FORCE SYSTEMS COMMAND
UNITED STATES AIR FORCE
HANSCOM AIR FORCE BASE, MASSACHUSETTS 01731


88 2 12 05 7

"This technical report has been reviewed and is approved for publication."


JAMES F. LEWKOWICZ
Contract Manager


HENRY A. OSSING
Chief, Solid Earth Geophysics Branch

FOR THE COMMANDER


DONALD H. ECKHARDT
Director
Earth Sciences Division

This report has been reviewed by the ESD Public Affairs Office (PA) and is releasable to the National Technical Information Service (NTIS).

Qualified requestors may obtain additional copies from the Defense Technical Information Center. All others should apply to the National Technical Information Service.

If your address has changed, or if you wish to be removed from the mailing list, or if the addressee is no longer employed by your organization, please notify AFGL/DAA, Hanscom AFB, MA 01731. This will assist us in maintaining a current mailing list.

Do not return copies of this report unless contractual obligations or notices on a specific document requires that it be returned.

Unclassified

SECURITY CLASSIFICATION OF THIS PAGE

REPORT DOCUMENTATION PAGE

1a. REPORT SECURITY CLASSIFICATION Unclassified		1b. RESTRICTIVE MARKINGS	
2a. SECURITY CLASSIFICATION AUTHORITY		3. DISTRIBUTION/AVAILABILITY OF REPORT Approved for public release Distribution unlimited	
2b. DECLASSIFICATION/DOWNGRADING SCHEDULE		5. MONITORING ORGANIZATION REPORT NUMBER(S) AFGL-TR-87-0264	
4. PERFORMING ORGANIZATION REPORT NUMBER(S)		7a. NAME OF MONITORING ORGANIZATION Air Force Geophysics Laboratory	
6a. NAME OF PERFORMING ORGANIZATION University of California	6b. OFFICE SYMBOL (If applicable)	7b. ADDRESS (City, State and ZIP Code) Hanscom Air Force Base Massachusetts 01731	
6c. ADDRESS (City, State and ZIP Code) Geology and Geophysics University of California Berkeley, California 94720		9. PROCUREMENT INSTRUMENT IDENTIFICATION NUMBER F19628-85-K0025	
8a. NAME OF FUNDING/SPONSORING ORGANIZATION DARPA	8b. OFFICE SYMBOL (If applicable) DARPA/GSD	10. SOURCE OF FUNDING NOS.	
8c. ADDRESS (City, State and ZIP Code) 1400 Wilson Blvd. Arlington, Virginia 22209		PROGRAM ELEMENT NO. 61101F	TASK NO. DA
11. TITLE (Include Security Classification) Regional Studies with Broadband Data		PROJECT NO. 5A10	WORK UNIT NO. AC
12. PERSONAL AUTHOR(S) McEvilly, Thomas V., Johnson, Lane R.			
13a. TYPE OF REPORT Final Report	13b. TIME COVERED FROM 2/13/85 TO 5/12/87	14. DATE OF REPORT (Yr., Mo., Day) 1987 August 29	15. PAGE COUNT 72
16. SUPPLEMENTARY NOTATION			
17. COSATI CODES		18. SUBJECT TERMS (Continue on reverse if necessary and identify by block number)	
FIELD	GROUP	SUB. GR.	
		explosions, Nevada Test Site, moment tensor reduced displacement potential	
19. ABSTRACT (Continue on reverse if necessary and identify by block number)			
Broadband seismic waveform data recorded in the distance range of 1 to 11 km from two underground explosions detonated at Pahute Mesa of the Nevada Test Site have been used to estimate the source time functions for the second-order moment tensors of these events. Data were available from 8 three-component stations for the explosion Harzer and from 11 stations for the explosion Chancellor. Stable moment tensor estimates with a good signal-to-noise ratio were obtained in the frequency range of 0.2 to 5.0 Hz. The moment tensors are dominated by the diagonal elements, but a significant asymmetry is present, with vertical force couples having a different time dependence than the horizontal force couples. When the isotropic parts of the moment tensors are interpreted as reduced displacement potentials the results are in reasonable agreement with theoretical and empirical models, although the parameters which are estimated with these models show systematic differences from published scaling relationships. These differences may be related to the fact that the explosions were detonated in unsaturated materials or			
20. DISTRIBUTION/AVAILABILITY OF ABSTRACT UNCLASSIFIED/UNLIMITED <input checked="" type="checkbox"/> SAME AS RPT. <input type="checkbox"/> DTIC USERS <input type="checkbox"/>		21. ABSTRACT SECURITY CLASSIFICATION Unclassified	
22a. NAME OF RESPONSIBLE INDIVIDUAL James F. Lewkowicz		22b. TELEPHONE NUMBER (Include Area Code) (617) 377-3028	22c. OFFICE SYMBOL AFGL/LWH

to the effects of spall in surficial layers above the source.

Source Characteristics of Two Underground Nuclear Explosions

Lane R. Johnson

Center for Computational Seismology, Lawrence Berkeley Laboratory,
and Department of Geology and Geophysics, University of California,
Berkeley, California 94720

ABSTRACT

Broadband seismic waveform data recorded in the distance range of 1 to 11 km from two underground explosions detonated at Pahute Mesa of the Nevada Test Site have been used to estimate the source time functions for the second-order moment tensors of these events. Data were available from 8 three-component stations for the explosion Harzer and from 11 stations for the explosion Chancellor. Stable moment tensor estimates with a good signal-to-noise ratio were obtained in the frequency range of 0.2 to 5.0 Hz. The moment tensors are dominated by the diagonal elements, but a significant asymmetry is present, with vertical force couples having a different time dependence than the horizontal force couples. When the isotropic parts of the moment tensors are interpreted as reduced displacement potentials the results are in reasonable agreement with theoretical and empirical models, although the parameters which are estimated with these models show systematic differences from published scaling relationships. These differences may be related to the fact that the explosions were detonated in unsaturated materials or to the effects of spall in surficial layers above the source.

Accession For	
NTIS CRA&I	<input checked="" type="checkbox"/>
DTIC TAB	<input type="checkbox"/>
Unannounced	<input type="checkbox"/>
Justification	
By	
Distribution	
Availability Codes	
Dist	Special
A-1	



1. INTRODUCTION

Although it would appear to be a relatively simple problem, there is still much that is not understood about the generation of elastic waves by large underground explosions. In general the seismograms produced by such explosions are considerably more complicated than what one would expect for a simple model, such as a pressure pulse applied to the interior of a spherical cavity in a homogeneous halfspace. Part of the difficulty may be related to the fact that the explosions are detonated in media which are heterogeneous in terms of both physical properties and preexisting stresses and there is dynamic interaction between the explosion and these heterogeneities, including the free surface. Also contributing to the difficulty is the media which lies between the source region and the receiver where the waves are recorded, for this media is generally heterogeneous and the associated wave propagation effects can add considerable complexity to the seismograms. It would appear that the first step in *striving to obtain a better understanding of the explosions source process* is to remove as much as possible of the wave propagation effects due to the intervening media between source and receiver.

An objective of the present study is to obtain unobstructed estimates of the source processes of large underground explosions. Such estimates are obtained through the method of moment tensor inversion in which calculated Green functions are used to remove propagation effects and the source is characterized in terms of the second-order moment tensor, a fairly general mathematical representation of spatially localized seismic sources. Having obtained estimates of the second-order moment tensor, these can be interpreted in terms of the physical processes in the source region, which is a second objective of the study.

The existence of numerous waveform data, previous studies in the same area, and an accurate velocity model all combine to make Pahute Mesa a convenient site for the present study. Pahute Mesa, a portion of the Nevada Test Site, has been the location

of numerous underground nuclear explosions in the past and continues to be an active location for the detonation of buried explosions. A large amount of ground motion data have been collected from these explosions, with numerous recordings at local, regional, and teleseismic distances. These data have been the subject of several scientific investigations which provide useful background information and also provide results which can be compared with those of the present study. Some of these previous studies of particular interest include Helmberger and Hadley (1981), Stump and Johnson (1984), Barker et al. (1985a, 1985b), and Patton (1985). The results of the moment tensor inversion method depend critically upon the availability of accurate Green functions and this requires that an accurate velocity model be available. A recent study by Leonard and Johnson (1987) has provided such a model for Pahute Mesa.

The data used in the present study were all recorded within 11 km of the explosion epicenters. There are certain advantages of using data from these close distances. First, many propagation effects, both elastic and inelastic, can be minimized by remaining as close as possible to the source. This can be important when trying to recover source information at the high frequencies where attenuation and scattering can have significant effects. Second, at these distances the seismograms contain P and S phases which left the source travelling in both upward and downward directions as well as both Rayleigh and Love surface waves. Thus the focal sphere is sampled fairly well, with the major gap in coverage being the P waves that leave the source region travelling downward at small angles of incidence and emerge at teleseismic distances.

2. DATA

The explosions Harzer and Chancellor were both detonated in Area 19 of Pahute Mesa at the Nevada Test Site. The parameters of these events are listed in Table 1. Note that the two events are only separated by 4.3 km and the shot environments are similar.

Ground motion recordings at near distances to these events were obtained with triggered digital event recorders. Each instrument package consisted of three force-balance accelerometers oriented to record radial, transverse, and vertical ground motion. The data were recorded at 200 samples per second with a resolution of 12 bits per sample and the complete system was flat to acceleration between frequencies of 0.2 and 50 Hz. The signal-to-noise ratio generally attains a maximum of about 1000 in the frequency band of 1 to 10 Hz, but decreases at both lower and higher frequencies. Because the recording instruments were accelerometers, this ratio falls to a value of 1 at a frequency of about 0.2 Hz, which means that periods longer than 5 sec are not well resolved in these data.

The locations of the two events and recording sites are shown in Figure 1. Data were obtained at 8 different stations for Harzer and at 11 stations for Chancellor. The station distances, azimuths, and elevations are listed in Tables 2 and 3 along with the maximum accelerations. Both experiments were conducted within the confines of Silent Canyon Caldera, a thick section of Cenozoic volcanic sediments.

The process of estimating the moment tensor from far-field acceleration recordings requires that three numerical integrations be performed. To ease this process somewhat, the acceleration data were first converted to velocity data by applying one numerical integration before beginning the inversion procedure. The knowledge that the long-time velocity level must return to zero prevents base-line uncertainties from causing any serious problems with this integration.

Previous studies employing similar ground motion data from Pahute Mesa (McLaughlin et al., 1983) have shown that spatial coherence of the waveforms over distances of a few hundred meters decreases significantly for frequencies above 5 Hz. Because of this and the fact that it is difficult and expensive to calculate Green functions at high frequencies, the data were low-pass filtered with a two-pole corner at 10 Hz and then decimated by a factor of 4 so as to reduce the Nyquist frequency from 100 Hz to 25 Hz.

The first ten seconds of velocity data for the Harzer and Chancellor events are shown in Figures 2 and 3, respectively, with the stations arranged in order of increasing epicentral distance. The records are fairly simple and of short duration at short distances but both the complexity of the records and their duration increase with distance. Inspection of the records at the closest distances is sufficient to establish that the duration of the source time function is less than 5 sec for the frequency band contained in these records. The first motion on the radial and vertical components are in the same direction at all stations, away and up, which is expected for a simple explosive source. More surprising are the transverse components, which have maximum amplitudes comparable to those on the radial and vertical components and at some stations have impulsive first arrivals at the time of the direct P wave, which is not expected for a simple explosive source. The first motions on the transverse components have mixed polarities (Tables 2 and 3) but a systematic lobed radiation pattern is not apparent. Although the scatter is considerable, the amplitudes on all three components decrease roughly as the inverse epicentral distance to the first power.

There is considerable evidence present in the seismograms of Figures 2 and 3 which indicates that either the source radiation pattern changes rapidly with azimuth or that local effects near the recording sites can significantly influence the waveforms. For instance, stations H1 and H3 are separated by only 0.1 km in range and 64 deg in azimuth yet have markedly different waveforms on all three components. Stations H6

and H8 show the same type of disparity. A comparison of the records from H5 and C4 tends to favor the hypothesis of a recording-site effect, because these stations, which were about the same distances from the two explosions and located at sites within 1 km of each other, show strong similarities in waveforms.

Station H3 had a partial malfunction in the field which caused the signal recorded on magnetic tape to have a very small amplitude. Through special steps taken in the laboratory it was possible to recover the records shown in Figure 2, which appear to be acceptable in the time domain. However, when these records are inspected in the frequency domain they show a signal-to-noise ratio at low frequencies which is an order of magnitude worse than the records recorded at other stations. This could have a strong effect upon a moment tensor inversion which is performed in the frequency domain, so the records from station H3 were not included in any of the moment tensor inversions.

3. RESULTS

3.1. Moment Tensor Inversions

The procedure used to estimate the moment tensors of the two explosions follows that outlined by Stump and Johnson (1977, 1984). The basic assumption involved in this procedure is that the source can be represented by a second-order force moment tensor and that higher order terms can be ignored. This would appear to be a valid assumption for explosions, since at least the initial size of the source is small compared to the wavelengths of interest. The inversions are performed in the frequency domain where the relation between the waveform data and the moment tensor elements is linear. No assumptions are invoked with regard to any relationships between the amplitudes of the various moment tensor elements or their time functions. The inversions were achieved through a least-squares minimization of the difference between

observed and predicted seismograms. The equations of condition were solved by singular value decomposition.

Critical to the moment tensor inversions are the Green functions which are used to remove propagation effects from the seismograms. The accuracy of the final results is directly related to the accuracy of the Green functions which depends upon having available a good model of the velocity and density structure. Leonard and Johnson (1987) have recently produced estimates of the average P and S-wave velocity structure in the shallow crust of Silent Canyon Caldera. These results differ from previous ones primarily in that velocities are modeled as continuous functions of depth rather than a series of constant velocity layers. The density measurements from borehole sampling plus the results in Snyder and Carr (1984) were used to associate a density model with the velocity models. The final results for the upper 4 km of the Silent Canyon Caldera are shown in Figure 4. Also shown in Figure 4 are estimates of anelastic properties which were used in the calculations. No direct measurements of these properties were available, so the estimates were based primarily on previous experience with shallow deposits (Johnson and Silva, 1981). The quality factor for S waves ranges from a value of 30 at the surface to a value of 75 at a depth of 4 km, while the quality factor for P waves ranges from 50 to 150 over the same range. Note that these quality factors should be interpreted to include both the effects of intrinsic attenuation and scattering, as the latter effect appears to be significant at high frequencies in the Silent Canyon Caldera (McLaughlin et al., 1983).

It should be noted that the Green functions of this study were calculated using a single one-dimensional model of the shallow structure at Pahute Mesa. This does not imply that such a model is completely appropriate for this region. In fact, there exists considerable geological and seismological evidence to indicate that appreciable lateral heterogeneity may be present in the Silent Canyon Caldera (Leonard and Johnson, 1987). The variations in waveforms in Figures 2 and 3 which were discussed above

support this inference. Thus an argument can be made for the use of a three-dimensional model for the calculation of the Green functions or at least for the use of a different suitably averaged one-dimensional structure for each source-receiver combination. However, the information necessary to construct such detailed velocity and density models of the three-dimensional structure are not available and not likely to become available in the near future. In such a situation one must appeal to some type of statistical averaging approach in order to mitigate the effects of the lateral heterogeneity. By including a sufficient number of seismograms recorded over a wide range of distances and azimuths and assuming that waveform effects due to the lateral heterogeneity will contribute to the moment tensor inversion in an incoherent manner while waveform effects due to the average one-dimensional structure will contribute in a coherent manner, one reasons that inaccuracies in the Green functions due to lateral heterogeneity may not all be translated directly into inaccuracies in the estimated moment tensors. While such an approach is definitely not as good as having more accurate Green functions, it does appear to give reasonable results. In effect, one is trading off inaccuracies in the Green functions against the number of seismograms used in the inversion in the hope that effects due to the lateral heterogeneity (or any other inaccuracies in the problem) will cancel themselves out in a random manner. While in principle the inverse problem of estimating the 6 elements of the moment tensor is completely determined given 6 seismograms (Stump and Johnson, 1977), in applications with real data it has been found that about 15 seismograms are generally required to insure stable results. Thus, in this study 21 seismograms are used to estimate the moment tensor for Harzer and 33 are used for Chancellor.

The Green functions were calculated by fairly standard methods that follow the general outline of Kind (1978). The stress-displacement boundary conditions were solved in the frequency-wavenumber domain using the general method of Haskell (1953) with suitable high frequency modifications as described by Harkrider (1964).

The inverse frequency and wavenumber transforms were performed with the trapezoid rule using a sampling rate in frequency governed by the Nyquist frequency of 25 Hz and a sampling in wavenumber governed by the maximum distance and fastest velocities (Alekseev and Mikhailenko, 1980). Attenuation was included according to the method of Silva (1976). The continuous velocities and density of the model were approximated by constant property layers of thickness 50 m in the upper 1.5 km and 100 m at greater depths.

The moment tensor inversions were obtained using standard singular value decomposition techniques following the method described by Stump and Johnson (1977). Estimates of the moment tensor are obtained in the frequency domain but are also transformed back to the time domain for further analysis there. The inversions were actually performed for the moment-rate tensors and these were then numerically integrated to obtain the moment tensors. In order to provide sufficiently dense sampling in frequency and also avoid possible truncation and windowing effects, 20 sec of data were included in the inversion procedure. However, because the transient signals on the moment tensors were confined to the first couple of sec and because, as mentioned above, the signal-to-noise ratio is suspect at long periods, only the first five sec of the moment tensors have been analysed in the time domain part of this study.

The net result of the inversion procedure is a symmetric second-order tensor in which the 6 elements all have independent time histories. The moment tensor \mathbf{M} can be treated as a 3 by 3 matrix with elements M_{11} , M_{12} , ... M_{33} , where the coordinate system is chosen so that 1 denotes North, 2 denotes East, and 3 denotes down. To aid in the physical interpretation of this tensor it is helpful to decompose it into an isotropic part M_I and deviatoric part \mathbf{M}_D , with the definitions

$$\mathbf{M} = M_I \mathbf{I} + \mathbf{M}_D \quad (1)$$

where \mathbf{I} is a diagonal unity matrix,

$$M_I \equiv \frac{\text{trace } \mathbf{M}}{3} = \frac{(M_{11} + M_{22} + M_{33})}{3} \quad (2)$$

and

$$\mathbf{M}_D \equiv \mathbf{M} - M_I \mathbf{I} \quad (3)$$

The isotropic part can be associated with the symmetrical parts of the source in which there is only a change in volume, and this is the type of source expected for a simple explosion. The deviatoric part can be associated with asymmetrical effects of the source, such as are expected for dislocation models of faulting or asymmetrical parts of an explosion. The interpretation is further aided by analyzing the deviatoric part in terms of its eigenvalues and eigenvectors. These can be thought of as the net effective magnitudes and associated directions, respectively, of the principal forces acting in the source region. Note that this decomposition in terms of isotropic parts, deviatoric parts, and principal forces is performed independently at each instant of time.

Before proceeding to a discussion of the estimates of the moment tensors which emerged from the inversion process, it is worth considering a few details of the process itself. With a total of 21 seismograms for the Harzer event and 33 for Chancellor, the inversions were quite stable in a numerical sense. For instance, the ratio of largest to smallest eigenvalue in the singular-value decomposition, which can be used as an estimate of the condition number, ranged between 4 and 27 for Harzer and between 4 and 16 for Chancellor. The reliability of the inversion results depends on frequency and this is illustrated in Figure 5. Here we see typical results for the estimates of the moduli of the moment tensor elements and estimates of their standard errors, which were calculated by assuming that the noise in the input data was white. Note that the ratio of the moment tensor estimates to their standard errors are a maximum in the range of 1 to 5 Hz and decreases at both lower and higher frequencies. This is interpreted to mean that the reliability of the moment tensor elements is best in the 1 to 5 Hz range but deteriorates at frequencies outside this range.

As can be seen in Figure 5, the spectral patterns apparent in the moment tensors are quite similar for the two explosions, with Harzer having in general slightly higher spectral amplitudes. The M_{11} elements have reasonably well defined low frequency levels, corner frequencies near 2 Hz, and high frequency slopes between -2 and -3. The M_{22} elements, which are not shown, are similar to this. The M_{33} elements differ somewhat in that they have an additional low frequency peak in the 0.3-0.4 Hz range. The average deviatoric elements have spectral amplitudes that are about 5 times smaller than the isotropic elements, have corner frequencies near 0.4 Hz, and have high-frequency slopes of about -2. The significance of these spectral differences in the elements of the moment tensors will be discussed more completely later in the paper.

Another way of evaluating the moment tensor elements is to consider how well they explain the data. Such results are shown in Figures 6 where the observed seismograms are compared with predicted seismograms calculated by convolving the Green functions with the estimated moment tensors for two of the Chancellor stations. The seismograms from C3 at an epicentral distance of 2.1 km are quite compact in time with the direct P and S phases having the largest amplitudes, and the estimated moment tensor for Chancellor does a good job of explaining all of the major features on the seismogram. The correlation coefficients between the observed and calculated seismograms for the radial, transverse, and vertical components are, respectively, 0.91, 0.86, and 0.81. The seismograms for station C7 at an epicentral distance of 9.8 km in Figure 6 are typical of the results at larger distances where the seismograms are more extended in time with both surface waves and scattered body waves undoubtedly accounting for part of the energy. The estimated moment tensor does a reasonably good job of explaining the first 4 sec of the radial and vertical components where the direct body waves are expected to arrive, but does poorly for later times on these components and does poorly for all times on the transverse components. The correlation coefficients between the observed and calculated seismograms are 0.41, 0.26, and 0.24

for, respectively, the radial, transverse, and vertical components. Considering all of the Harzer seismograms, the average correlation coefficient is 0.63 ± 0.22 for the radial components, 0.40 ± 0.30 for the transverse components, and 0.44 ± 0.22 for the vertical components. Similar average correlation coefficients for the Chancellor seismograms are 0.48 ± 0.30 , 0.23 ± 0.40 , and 0.37 ± 0.32 . While correlation coefficients are insensitive to absolute amplitudes, Figure 6 shows that the observed and calculated amplitudes are in reasonable agreement on the radial and vertical components, with a slight tendency for the calculations to underestimate at short distances and overestimate at larger distances. The transverse component is consistently underestimated at all distances. Thus, on the average, the radial components are fit best, the transverse components are fit worst, and Harzer is fit better than Chancellor.

Based on these results showing the ability of the moment tensors to fit the observed data, a plausible interpretation is that the inversion process is successful in fitting the early parts of the seismograms where the arrivals are direct body waves which are likely to be consistent with the Green functions, and the process is also successful in ignoring some of the large amplitudes during the later parts of the seismogram which are not consistent with the Green functions and are most likely due to scattering and multi-pathing. Experience indicates that this type of success is dependent on having a large number of seismograms so that the problem is highly over-determined. As the number of seismograms used in the inversion process decreases, the likelihood increases that a random phase on a particular seismogram will be interpreted as part of the source time function. It follows that the ability to fit the observed seismograms may actually improve as the number of seismograms used in the inversion process is decreased. An implication of this interpretation is that good agreement between the observed and fitted seismograms is not necessarily an indication that the moment tensor estimates are accurate.

While the moment tensors are actually estimated in the frequency domain, both amplitude and phase are available so that the results can be easily transformed to the time domain, where the interpretation is often more straightforward. The first five seconds of the moment tensors which were estimated for the explosions Harzer and Chancellor are shown in Figures 7 and 8, respectively. Several general observations apply to the results for both Harzer and Chancellor. The diagonal elements of the moment tensors dominate and are qualitatively similar in both their magnitudes and time histories. They are basically slightly acausal step functions with rise times of less than 1 sec. There is discernable overshoot on all of the diagonal elements but this effect is most developed on the M_{33} elements. On the other hand, the off-diagonal elements are smaller in magnitude than the diagonal elements and more variable in their time histories. In general, they are more emergent and appear to have less high-frequency content than the diagonal elements. Their onset is generally delayed with respect to the onset of the diagonal elements.

The differences between the isotropic and deviatoric parts of the moment tensors displayed in Figures 7 and 8 are consistent with the spectral data of Figure 5. There is a suggestion in these spectral data that two separate functions might be present in the sources. The first is a low frequency function with a corner frequency near 0.4 Hz and a spectral slope less steep than -2 which is present in both the isotropic and deviatoric parts. The second is a higher frequency function with a corner frequency near 2.0 Hz and a spectral slope more steep than -2 which is present only in the isotropic part of the moment tensors. Further inspection of the spectra of the individual elements of the moment tensor indicates that the relative amplitude of the low frequency function is larger on the M_{33} elements than on the M_{11} and M_{22} elements. These results are entirely consistent with the time-domain plots in Figures 7 and 8 where it is clear that the M_{11} and M_{22} elements are more similar to each other than they are to the M_{33} elements and that the M_{33} elements have additional low frequency energy.

3.2. Isotropic Moment Tensor

The primary concern of this paper is the isotropic part of the moment tensor, which is defined here in terms of the trace of the moment tensor (Equation 2). As mentioned in the previous section, this is the part of the source which is related to a change of volume and it is the only part of the source which is nonzero for an ideal explosion. The isotropic sources which were estimated for the two events Harzer and Chancellor are shown in both the frequency and time domain in Figure 9. The results are quite similar for the two events. In the time domain these isotropic parts are fairly simple, showing slightly acausal one-sided pulses that rise to a peak within 1 sec and then fall to a constant nonzero level. In the spectral domain they show high-frequency slopes in the -2 to -3 range, spectral corners at about 2 Hz, and additional peaking in the spectra in the 0.3-0.4 Hz range. This peaking in the spectra below 1 Hz tends to obscure the corner frequency at higher frequency, particularly in the case of Harzer. The interpretation of these results is facilitated by comparing them with the predictions of various theoretical and empirical models of explosive sources.

In dealing with explosive sources it is convenient to consider a scalar potential $\Psi(t)$ which is called the reduced displacement potential. In a homogeneous elastic medium the vector displacement \mathbf{u} at any time t and position \mathbf{x} is simply

$$\mathbf{u}(t, \mathbf{x}) = -\nabla \left[\frac{\Psi(t - \mathbf{x}/\alpha)}{\mathbf{x}} \right] \quad (4)$$

where α is the velocity of P waves. Because of this simplicity, much of the previous work on explosive sources has been expressed in terms of the reduced displacement potential. There also exists the following simple relationship between the reduced displacement potential and the isotropic part of the moment tensor

$$M_I(t) = 4\pi\rho\alpha^2\Psi(t) \quad (5)$$

where ρ is density. Thus the estimates of the isotropic parts of the moment tensor

which have been obtained in this study can also be interpreted as estimates of the reduced displacement potential.

The reduced displacement potential is often described by parameterized models and several different parameterizations have been suggested. Mueller and Murphy (1971) considered the analytical solution for a pressure pulse acting on the interior of a spherical cavity and introduced the elastic radius of the source and the pressure acting at that radius as parameters. The characteristic time for this source is the elastic radius divided by the velocity of compressional waves. Haskell (1967) introduced an empirical relationship of the form

$$\Psi(t) = \Psi_{\infty} \left[1 - f(t/\tau) \right] H(t) \quad (6)$$

with

$$f(t) = e^{-t} \left[1 + t + c_2 t^2 + c_3 t^3 + c_4 t^4 \right] \quad (7)$$

and where τ is a characteristic time of the source, Ψ_{∞} is the long-time response, and H is a unit step function. Haskell proposed that $c_2=1/2$, $c_3=1/6$, and c_4 be an adjustable parameter. von Seggern and Blandford (1972) suggested an expression of the same form but with $c_3=c_4=0$ and c_2 an adjustable parameter. Helmberger and Hadley (1981) also adopted the same form and proposed that $c_2=1/2$, $c_4=0$, and c_3 be an adjustable parameter. Thus we have four different functions available for describing the reduced displacement potential and each functional has 3 adjustable parameters. In all cases two of these parameters are the characteristic time τ and the long-time level Ψ_{∞} . For the Mueller-Murphy model the third parameter is the ratio of peak pressure to constant pressure at the elastic radius, while for the other three models is is one of the constants in equation 7.

The isotropic parts of the estimated moment tensors shown in Figure 9 were each interpreted in terms of the four different models of the reduced displacement potential that are described in the previous paragraph. The various models were fit to the

observational data by adjusting the parameters of the model until what appeared to the eye as a reasonable fit was achieved in the time domain. In essence, the characteristic time τ was determined by fitting the rise time of the first pulse, Ψ_{∞} was determined by fitting the amplitude of the first pulse, and the third parameter was determined by fitting the ratio of the peak amplitude to the amplitude in the interval of 4-5 sec. The results of this fitting process are shown in both the time and frequency domain in Figures 10-13 and the parameters used to obtain these fits are given in Table 4.

For frequencies less than 1 Hz, all four models for the reduced displacement potential can be fit to the isotropic part of the moment tensor so as to satisfactorily explain the major features of the isotropic moment tensors of Harzer and Chancellor (Figures 10-13). For frequencies above 1 Hz, there are distinct differences between the abilities of the models to fit the data. The Harzer data can be fit better than the Chancellor data in both the time and frequency domains. The Mueller-Murphy model does slightly better than the other models in fitting the Harzer time function (Figure 10), particularly for the back side of the first pulse between 1 and 2 sec. In the frequency domain both the Mueller-Murphy and von Seggern-Blandford models, which have high-frequency slopes of -2, fit the Harzer data quite well, while the Haskell model with a -4 slope and the Helmberger-Hadley model with a -3 slope underestimate the high frequency energy in the observational data. For Chancellor there are short-period fluctuations in the estimated time function between 1 and 4 sec which vaguely suggest the possibility of a multiple event. None of the models can fit these fluctuations and all of the models underestimate the high-frequency energy in the Chancellor observed spectrum, particularly in the 1 to 5 Hz range. The high-frequency slope of the Chancellor spectrum is between -2 and -3, which can be explained by the Mueller-Murphy, von Seggern-Blandford, and Helmberger-Hadley models but not by the Haskell model. Recalling the earlier suggestion that both a low-frequency function and a high-frequency function may be present in the isotropic part of the moment

tensors, it is apparent in Figures 10-13 that the process of fitting the models to observational data in the time domain has given preference to the low-frequency function. This is particularly evident in the Chancellor spectral plots, where the high-frequency function with a corner frequency near 2 Hz is poorly fit by the models.

Turning now to the model parameters which were estimated during the fitting process (Table 4), we see that the values of these parameters can depend upon the model. The estimates for Ψ_{∞} and τ show variations of about 10% and 30%, respectively, between the four models. The pattern is consistent for τ , with models having steeper high-frequency slopes requiring shorter characteristic times. This model dependent variation of 30% in τ could lead to significant differences if τ were used to infer an elastic radius. In a relative sense all four models show a similar pattern in that Harzer has a Ψ_{∞} which is about 25% greater than for Chancellor and a τ which is about 50% greater.

3.3. Deviatoric Moment Tensor

The moment tensor of an ideal explosion would have only an isotropic part with all deviatoric parts equal to zero. This is not the case for either of the events Harzer or Chancellor, as can be readily observed in Figures 5, 7, and 8 where diagonal elements are not all identical and off-diagonal elements are not all zero. Even more basic evidence concerning the existence of the deviatoric elements can be inferred from the strong early-arriving energy which is present on the transverse components in Figures 2 and 3, because an ideal explosive source in a plane-layered isotropic medium should generate no transverse components. In fact, noting that the transverse components of ground motion are comparable in amplitude to the radial and vertical, it is surprising that the off-diagonal elements of the estimated moment tensors (Figures 7 and 8) are so much smaller than the diagonal components. What appears to be happening is that, either because they are incompatible with the radial and vertical components or

because they are generated by a mechanism which is not incorporated in the calculation of the Green functions, the transverse components of ground motion have a disproportionately small effect upon the estimated moment tensors. In support of this interpretation, note that in Figure 6 the observed transverse seismograms are consistently underestimated by the seismograms calculated with the estimated moment tensors.

The deviatoric moment tensor (Equation 3) is a symmetric second-rank tensor and is conveniently interpreted in terms of its 3 eigenvalues and the directions of the corresponding eigenvectors. Corresponding to the usual interpretation of principal axes of fault-plane solutions, these eigenvalues and eigenvectors have been identified with the tensional principal axis T, intermediate principal axis I, and pressure principal axis P. This eigenvalue decomposition of the deviatoric moment tensor as a function of time is shown in Figure 14 for both Harzer and Chancellor.

The tensional and pressure deviatoric eigenvalues in Figure 14 are only slightly smaller in amplitude than the isotropic elements in Figure 9. In the case of Harzer the intermediate eigenvalue is close to zero throughout the first 5 sec so the mechanism for this part of the source is consistent with a simple shear dislocation. This also means that the tensional and pressure eigenvalues are mirror images of each other with respect to their time histories. This time dependence of the tensional and pressure eigenvalues shows a general similarity to the isotropic element in Figure 9. Closer inspection reveals that the deviatoric eigenvalues are delayed in time by about 0.5 sec with respect to the isotropic element and have longer rise times of about 1.5 sec for the first pulse as compared to about 1.0 sec on the isotropic element. In the case of Chancellor the intermediate eigenvalue departs from zero after about 1 sec, which may indicate a source mechanism more complicated than a simple shear dislocation, and this causes the tensional and pressure eigenvalues to differ somewhat in their time histories. However, there is still a general similarity between the tensional and pressure

eigenvalues and the isotropic element in Figure 9. As in the case of Harzer, the deviatoric eigenvalues are delayed by about 0.5 sec with respect to the isotropic element and have slightly longer rise times for the first pulse.

Referring to Figures 7 and 8, one can see that the size and time histories of the deviatoric eigenvalues arises primarily from the differences between the diagonal elements of the moment tensor rather than the amplitudes of the off-diagonal elements. Further inspection reveals that for both Harzer and Chancellor the major cause of the deviatoric parts of the moment tensors is the fact that starting about 0.5 sec after the origin time the M_{33} elements begin to differ significantly from the M_{11} and M_{22} elements. This explains why the the first large pulse on the deviatoric eigenvalues is delayed with respect to the first large pulse on the isotropic elements.

While Figure 14 describes the eigenvalues of the deviatoric parts of the moment tensors, Figure 15 describes the eigenvectors. These are displayed by plotting on a stereographic net the directions of the eigenvectors as a function of time. As these directions can be quite unstable when the eigenvalues are small, the eigenvectors are plotted only for the time interval 0.5-3.0 sec when the eigenvalues have large values and should be least affected by noise. A simple physical interpretation of the eigenvector directions in Figure 15 is not obvious. Initially the P axis is near the horizontal which could be interpreted as strike-slip motion on a fault plane striking northwest, and this roughly corresponds to the types of tectonic stress release that others have found for Pahute Mesa explosions (Wallace, et al. 1983, 1985; Lay et al., 1984). As time progresses however, the P axis rotates toward the vertical, which could indicate a transition from predominantly strike-slip to predominantly dip-slip motion. Given the lack of an obvious simple pattern in the direction of the eigenvectors, the fact that the deviatoric elements result primarily from differences between the larger diagonal elements of the moment tensors, and the fact that these elements have a spectral content which is shifted toward the low frequencies where the signal-to-noise ratio is worse,

considerable uncertainty must be attached to the interpretation of the deviatoric parts of these moment tensors.

4. INTERPRETATION

The moment tensor of an ideal explosion has only diagonal elements and these three elements all have the same time function. The moment tensors which have been estimated for Harzer and Chancellor are dominated by the diagonal elements, but they do not all have identical time functions. In particular, the M_{33} elements are significantly different from the M_{11} and M_{22} elements. Assuming that the explosion began as an isotropic source of a pressure pulse in an approximately spherical cavity, the conclusion follows that the medium has responded to this pressure pulse in an asymmetric manner, with the response in the vertical direction being different from that in the horizontal directions. There are a number of reasons why such an asymmetric effect might be expected for events such as Harzer and Chancellor, such as the vertical effects of gravity, the strong vertical gradient in material properties, and the fact that discontinuities in material properties are predominantly horizontal, which includes the free surface. A basic question is whether these asymmetric properties of the medium are sufficient to explain the asymmetric effects which are observed in the moment tensor.

An effect which could possibly explain the asymmetry of the Harzer and Chancellor moment tensors is the phenomenon known as spall. For buried explosions this effect is caused primarily by the direct compressional wave being reflected from the free surface with a change in sign, which can result in tensional stresses at particular depths, nonlinear failure, part of the material separating in ballistic flight, and a delayed impact when this material rejoins the rest of the earth. Day et al. (1983) have modeled spall by a system of vertical forces in which momentum is conserved. Stump (1985) has elaborated upon this model and has shown that for high-frequency

waveforms observed near the source the contribution from the spall can be comparable in amplitude to that from the explosion. The spall model of Day et al. (1983) consists entirely of vertical forces which require different Green functions from the ones used for the force couples of the second-order moment tensor elements. However, Stump (1988) has shown by forward modeling that the Green functions for the vertical force are practically indistinguishable from a combination of the Green functions of the diagonal elements of the moment tensor. If $e(t)$ is the time function of the explosion and $s(t)$ is the integrated time function of the forces associated with the spall, then Stump (1987) suggests that

$$\begin{aligned}
 M_{11} &= e(t) + s(t) \\
 M_{22} &= e(t) + s(t) \\
 M_{33} &= e(t) + 2s(t)
 \end{aligned}
 \tag{8}$$

If spall is modelled as a horizontal tension crack, then expressions similar to equation 8 are obtained except that the factor 2 in the M_{33} term becomes $\frac{\lambda+2\mu}{\lambda}$, which has a value of 2.9 at the depth of the explosions and slightly higher values at shallower depths. Both of these results suggest that the presence of spall is consistent with the observation that the M_{33} elements of the moment tensors are different from the M_{11} and M_{22} elements.

Spall is commonly observed to occur with shallow events such as Harzer and Chancellor, and for the case of Harzer there is considerable quantitative information available concerning the details of the process. Patton (1985) has studied the Harzer spall process using data from in situ measurements, pictures of the ground surface, and computer simulations. He finds that spall for this event was a fairly symmetrical process, beginning at a depth of 290 m about 0.3 sec after the origin time of the explosion and extending out to a radial distance of about 1.3 km. The ballistic period at ground zero was between 0.9 and 1.7 sec, with this range in interval most likely due to

multiple spall in the surficial layers. Patton calculates the momentum of the spall mass as $1.5 \cdot 10^{17}$ dyne-sec and finds that this accounts for between 25% and 60% of the total isotropic moment of the Harzer event, where the range depends upon the ballistic period assumed for the spall and the calculations were performed for the excitation of Lg waves in the frequency range of 0.2 to 0.5 Hz.

Referring to the moment tensor which was estimated for Harzer (Figure 7), the difference between the M_{33} element and the other diagonal elements is generally consistent with the spall process which has been outlined by Patton (1985). The anomaly on the M_{33} element is clearly present by 0.5 sec and lasts until about 2.5 sec, which corresponds roughly to the time period in which the spall process operated, particularly if one allows for the fact that the spall source may have had dimensions of 2-3 km. The sign of the anomaly changes from positive to negative slightly after 1 sec, which may correspond to the beginning of spall closure. The size of the anomaly is roughly 50% of the isotropic part of the total source, which is also consistent with Patton's estimate of the spall contribution. The same general interpretation can also be given for the estimated moment tensor for Chancellor, although in this case the effects of spall appear to be somewhat smaller than for Harzer and the corroborating information concerning the spall process is not available. Thus, on the basis of the data which are available, spall must receive serious consideration as a possible explanation of the asymmetry in the diagonal elements of the moment tensors.

One result of this study has been an estimate of reduced displacement potentials from the analysis of near-source waveforms (Figure 9). It is of interest to compare these results with other estimates of reduced displacement potentials, most of which have been based on free-field measurements at buried sites within a few hundred meters of the sources (Rodean, 1971, 1981; Mueller and Murphy, 1971). A method of making such comparisons is to use the parameters of Table 4 which have been obtained by fitting various models to the reduced displacement potentials. This is

particularly convenient for the Mueller-Murphy model because a fairly complete set of scaling relationships are available for this model (Mueller and Murphy, 1971; Murphy, 1977). Using the scaling relationship of Murphy (1977, Figure 15) the Ψ_{∞} estimated for Harzer and Chancellor are appropriate for m_b values of 5.25 and 5.15, respectively, which are about 0.25 less than the published values (Table 1). Stated in another way, the scaling relationship and the published m_b values predict Ψ_{∞} values of $4-8 \cdot 10^{10} \text{ cm}^3$ for Harzer and $3-6 \cdot 10^{10} \text{ cm}^3$ for Chancellor, which are about 2 to 3 times larger than the estimated values (Table 4). Thus, relative to scaling relationships based on the published m_b values, the reduced displacement potentials estimated for Harzer and Chancellor seem to be too small by a factor of at least 2. There are a couple of possible explanations for this discrepancy.

First note that the scaling relationships of Murphy (1977) are based primarily upon explosions in saturated tuff-rhyolite materials and the explosions Harzer and Chancellor, while they were in the same type of material, were located above the water table (Table 1). Murphy (1981) and Wallace and Barker (1987) have both found that explosions detonated in dry tuff and alluvium have coupling efficiencies that are two to three times less than explosions detonated in saturated tuff. In the case of Murphy (1981) this difference manifests itself in m_b values which are smaller than the saturated tuff predictions for a given yield and in the case of Wallace and Barker (1987) it manifests itself in estimated Ψ_{∞} values which are smaller than the saturated tuff predictions for a given yield. The yields of Harzer and Chancellor have not been announced so a direct comparison with these published results is not possible, but there is a general agreement if one assumes that the effect of dry material at the shot depth is to decrease Ψ_{∞} even more than m_b .

Secondly, it is important to recall that the parameters of Table 4 were determined by fitting the isotropic part of the moment tensor, which is only part of the complete moment tensor which was estimated. The m_b values represent the effect of the

complete moment tensor which is considerably more than just the isotropic part which is represented in the reduced displacement potential. Additional information is provided by Patton (1985) who used Rayleigh and Lg waves recorded at regional distances to estimate an isotropic moment M_I of $17 \cdot 10^{22}$ dyne-cm for the Harzer event, and went on to conclude that $7 \cdot 13 \cdot 10^{22}$ dyne-cm of this was due to the explosion and the rest was contributed by spall. These results can be compared to an average value of $7.4 \cdot 10^{22}$ dyne-cm from Table 4 for M_I of Harzer, which is about a factor two less than what Patton (1985) obtained. Note that the peak value of the spectrum for the Harzer isotropic moment has a value of about $20 \cdot 10^{22}$ dyne-cm at 0.3 Hz (Figure 9) but the models all have a peaked spectrum with a lower value of Ψ_∞ (Figures 10-13).

Another parameter of Table 4 which can be compared with scaling relationships available in the literature is the characteristic time τ . Using the scaling relationships of Murphy (1977, 1981) the m_b values of Harzer and Chancellor can be converted to predicted values of 0.14 sec and 0.12 sec, respectively, for the characteristic time τ . In Table 4 we find estimated values based on the Mueller-Murphy model of 0.55 sec and 0.35 sec, respectively, which are about three times larger than the predicted values. Once again it should be noted that the scaling relationships being used here were developed for explosions detonated in saturated tuff-rhyolite, so these differences may indicate that different scaling relationships are required for detonations in dry materials. Alternatively, it may mean that the depth dependence of the Mueller-Murphy scaling relationships is not appropriate for explosions above the water table. In a carefully controlled study of small chemical explosions Flynn and Stump (1988) found that as the depth of the explosion decreased the amount of high-frequency energy decreased more than predicted by the Mueller-Murphy scaling relationships, and they attribute this effect to the change from full to partial containment. The large characteristic times observed in this study are qualitatively consistent with the results of Flynn and Stump.

On the basis of the comparisons with published scaling relationships it appears that the reduced displacement potentials estimated in the present study have Ψ_{∞} values that are a factor of about 2 too small and τ values which are about a factor 3 too large. This may mean that the method of moment tensor inversion used in this study has systematically underestimated both the low-frequency amplitude and the high-frequency contributions to the explosive part of the source, or it may mean that the published scaling relationships can not be applied to explosions above the water table without modifications. A partial answer to this question is supplied by the results in Figure 16.

Figure 16 shows the observed seismograms and several different versions of predicted seismograms at the closest available site, station C10 at a distance of 1.8 km from Chancellor. The closest station was selected with the idea that it should have the minimum propagation effects and thus provide the most direct estimate of the source time function. The seismograms predicted by the complete moment tensor are shown in Figure 16 and the agreement is quite good, although the predicted amplitudes are slightly less than observed for the first arrival. Also shown in Figure 16 are the predicted seismograms which are obtained when only the diagonal elements of the moment tensor are included and when only the isotropic part of the moment tensor is included. By comparing these results with those for the complete moment tensor, one can see the progressive effects of removing the off-diagonal elements of the moment tensor and then removing the asymmetrical part of the diagonal elements. It is clear from this comparison that both of these nonisotropic effects in the moment tensor make significant contributions to the predicted seismograms, including the first arrival. Also shown in Figure 16 are the seismograms predicted by the Mueller-Murphy model of an explosion using the parameters of Table 4. For this model, which has a characteristic time of 0.35 sec, the predicted amplitudes are smaller than the observed amplitudes by a factor of 2-3 for the first arrival and the first downswing is not well modeled. Also shown are the predicted seismograms for a Mueller-Murphy model

with a characteristic time of 0.18 sec, which improves the agreement for both the amplitude and shape of the first arrival. Consideration of observed and predicted seismograms at greater distances leads to the same general result, that a characteristic time of 0.18 sec predicts the first arrival on the observed seismograms better than the value of 0.35 which was obtained by fitting the reduced displacement potential. Similar results were obtained for the other models of the reduced displacement potential which are listed in Table 4. This leads to the conclusion that, if a simple explosion were assumed for the source and only the first cycle on the radial and vertical components of ground motion were fit, then characteristic times would be obtained which would be only about half those listed in Table 4, which bring them into closer agreement with the published scaling relationships. On the other hand, if a complete moment tensor is used as the source model, one can obtain even better fits of the first arrival, do a much better job of fitting the later arrivals on the seismogram, and also fit the transverse components.

This discrepancy in characteristic times is related to the discussion of section 3.2 concerning the possibility that the moment tensors contain two distinct time functions, a low-frequency function which is strongest on the M_{33} element and which controls the modeling of the reduced displacement potentials, and a high-frequency function with a corner frequency near 2 Hz which was largely ignored in the fitting process. It now appears that the first arrivals on the seismograms are more closely related to the high-frequency function than to the low-frequency function. This could be interpreted to mean that the high-frequency function is associated with the explosion while the low-frequency function is associated with the spall process.

Putting all of the these results together, it is possible to describe a series of physical processes which, while certainly not unique, at least provide one plausible interpretation of the moment tensors which were estimated for Harzer and Chancellor. The events were detonated above the water table in unsaturated materials and spall was an

important part of the process, so that in effect these were only partially contained explosions. The spall effect contributed an asymmetry to the source, beginning at the latest a few tenths of a second after detonation, so that the effective forces in the vertical direction had different amplitudes and different time functions than those in the horizontal directions. The moment tensor estimates were constructed on the basis of the radiated seismic waveforms, and because none of the stations were at distances less than three source depths, all the processes in the immediate source area, including both the explosion and spall, were interpreted as being caused by a single effective source process. Thus the moment tensors contained the combined effects of these various processes, including the explosion which may have had characteristic times of as small as 0.1 sec and the spall which may have had characteristic times of as long as 1 sec or more. Extracting the isotropic part of the moment tensor helps isolate the explosive part of the source, but it is not completely successful because the spall process involves a change in volume and thus also appears in the isotropic part. It appears that the reduced displacement potentials which have been estimated in this study contain contributions from spall in addition to the explosive source, which results in a possible overestimation of the characteristic time of the explosion. The inelastic spall process absorbs energy which might have otherwise gone into seismic waves, resulting in a decreased seismic coupling coefficient and a reduced displacement potential which is smaller than what is usually obtained for fully contained explosions in saturated materials.

5. DISCUSSION

The problem of deciphering the physics of explosive sources from the study of radiated elastic waves has been separated into two different inverse problems in this study. The first inverse problem is to remove the propagation effects and obtain an estimate of the effective force system operating in the immediate vicinity of the source, which has been characterized by the second-order moment tensor. Unique solutions are possible for this inverse problem, and in the case of the explosions Harzer and Chancellor stable results were obtained in the frequency range of 0.2 to 5.0 Hz. This was possible because of the large number of well-distributed recording sites and the availability of a good estimate for the average velocity structure in the region of study. The second inverse problem consists of interpreting the moment tensor in terms of the physical processes acting in the source region. Solutions to this problem are inherently nonunique, so additional information and assumptions must generally be included in the interpretation process.

A basic result for the explosions Harzer and Chancellor is that the moment tensor is dominated by its diagonal elements but that these elements contain an important asymmetry, namely that the M_{33} element differs significantly from the M_{11} and M_{22} elements. Considerable evidence points to the possibility that this asymmetry is related to spall processes taking place in the depth interval between the explosion and the free surface. An interpretation in terms of a source which contains the effects of both a symmetric explosion and an asymmetrical spall is capable of quantitatively explaining many of the features of the moment tensor. For distances in the range of 1 to 11 km and frequencies in the range of 0.2 to 5.0 Hz, these two different source effects have comparable amplitudes and it is not easy to separate their relative contributions to the moment tensor. Thus, if the isotropic part of the moment tensor is interpreted as being due solely to a simple explosion, the results could be misleading.

The tentative conclusion that both the explosion and spall have made significant contributions to the radiated elastic waves which were analyzed in this study calls into question one of the basic assumptions of the method which was used, namely that the source is sufficiently localized in space so that it can be represented by a second-order moment tensor. It would appear that an inversion should be performed which takes into account the fact that two sources may be acting to two different locations, one at the detonation point of the explosion and the other at a shallower depth where spall is suspected. While this is possible, Stump (1988) has already performed numerical experiments for this type of inverse problem and the results are not promising. He finds that when the closest stations are several times the separation of the two sources, there is a strong trade-off between the two sources and the inversion is highly nonunique. Having observations from points closer to the sources might improve the situation but one then encounters another problem, that of interpreting ground motions in the nonlinear zone of the source where the basic wave equations which have been assumed throughout this study are no longer valid.

This paper has concentrated on the interpretation of the most prominent parts of the moment tensor, the diagonal elements. The deviatoric elements were also analyzed but a definitive interpretation could not be given. The events Harzer and Chancellor were both detonated in parts of Pahute Mesa where there have been numerous previous explosions and neither seemed to show evidence of strong tectonic release. It would be helpful if the same type of analysis used in this study could be applied to an explosion known to have significant tectonic release. It could be that, given the experience gained in studying the moment tensor from such an event, one could then return and give a more meaningful interpretation of the deviatoric elements of the Harzer and Chancellor explosions.

Finally, it should be pointed out that, while the transverse components of ground motion were included in the inversion, helped constrain the estimates of the moment

tensors, and were partially modeled by the predicted seismograms, they have not been satisfactorily explained. In fact, the interpretation in terms of a symmetric explosion and a vertical spall process predicts no transverse motion, a result obviously at variance with the observations of transverse motions comparable in amplitude to the radial and vertical motions at all distance ranges. Apparently, our understanding of the generation of elastic waves by explosions is still incomplete.

6. REFERENCES

- Alekseev, A. S., B. G. Mikhailenko, 1980. The solution of dynamic problems of elastic wave propagation in inhomogeneous media by a combination of partial separation of variables and finite-difference methods, *J. Geophys.*, 48, 161-172.
- Barker, J. S., S. H. Hartzell, L. J. Burdick, D. V. Helmberger, 1985a. Determination of effective source functions and measurement of seismic yields from underground nuclear explosions at Pahute Mesa by modeling near-field records, Final Technical Report WCCP-R-85-02, Woodward-Clyde Consultants, Pasadena.
- Barker, J. S., L. J. Burdick, T. C. Wallace, 1985b. Analysis of near-field seismic waveforms from underground explosions, Report AFGL-TR-85-0321, Air Force Geophysics Laboratory, Hanscom Air Force Base, ADA165227.
- Day, S. M., N. Rimer, J. T. Cherry, 1983. Surface waves from underground explosions with spall: analysis of elastic and nonlinear source models, *Bull. Seism. Soc. Am.*, 73, 247-264.
- Flynn, E. C., B. W. Stump, 1988. Effects of source depth on near source seismograms, in press, *J. Geophys. Res.*
- Harkrider, D. G., 1964. Surface waves in multilayered elastic media, Part I: Rayleigh and Love waves from buried sources in a multilayered elastic halfspace, *Bull. Seism. Soc. Am.*, 54, 627-679.
- Haskell, N. A., 1953. The dispersion of surface waves in multilayered media, *Bull. Seism. Soc. Am.*, 43, 17-34.
- Haskell, N. A., 1967. Analytic approximation for the elastic radiation from a contained underground explosion, *J. Geophys. Res.*, 72, 2583-2587.
- Helmberger, D. V., D. M. Hadley, 1981. Seismic source functions and attenuation from local and teleseismic observations of the NTS events Jorum and Handley, *Bull. Seism. Soc. Am.*, 71, 51-67.
- Johnson, L. R., W. Silva, 1981. The effects of unconsolidated sediments upon the ground motion during local earthquakes, *Bull. Seism. Soc. Am.*, 71, 127-142.
- Kind, R., 1978. The reflectivity method for a buried source, *J. Geophys.*, 44, 603-612.

- Lay, T., T. C. Wallace, D. V. Helmberger, 1984. The effects of tectonic release on short-period P waves from NTS explosions, *Bull. Seism. Soc. Am.*, 74, 819-842.
- Leonard, M. A., L. R. Johnson, 1987. Velocity structure of Silent Canyon Caldera, Nevada Test Site, *Bull. Seism. Soc. Am.*, 77, 597-613.
- McLaughlin, K. L., L. R. Johnson, T. V. McEvilly, 1983. Two-dimensional measurements of near-source ground accelerations, *Bull. Seism. Soc. Am.*, 73, 349-375.
- Mueller, R. A., J. R. Murphy, 1971. Seismic characteristics of underground nuclear detonations, Part I. Seismic spectrum scaling, *Bull. Seism. Soc. Am.*, 61, 1675-1692.
- Murphy, J. R., 1977. Seismic source functions and magnitude determinations for underground nuclear detonations, *Bull. Seism. Soc. Am.*, 67, 135-158.
- Murphy, J. R., 1981. P wave coupling of underground explosions in various geologic media, in *Identification of Seismic Sources - Earthquake or Explosion*, 201-203, E. S. Husebye and S. Mykkeltveit (eds), Reidel.
- Patton, H. J., 1985. Source models of the Harzer explosion from observations of regional surface waves and Lg, Lawrence Livermore National Laboratory, preprint.
- Rodean, H. C., 1971. *Nuclear-Explosion Seismology*, U.S. Atomic Energy Commission.
- Rodean, H. C., 1981. Inelastic processes in seismic wave generation by underground explosions, in *Identification of Seismic Sources - Earthquake or Underground Explosion*, 97-189, E. S. Husebye and S. Mykkeltveit (eds), Reidel.
- Silva, W., 1976. Body waves in a layered anelastic solid, *Bull. Seism. Soc. Am.*, 66, 1539-1554.
- Snyder, D. B., W. J. Carr, 1984. Interpretation of gravity data in a complex volcano-tectonic setting, southwestern Nevada, *J. Geophys. Res.*, 89, 10,193-10,206.
- Stump, B. W., 1985. Constraints on explosive sources with spall from near-source waveforms, *Bull. Seism. Soc. Am.*, 75, 361-377.

- Stump, B. W., 1988. Resolution of complex explosive source functions in the frequency domain, in press, Geophys. J. R. Astr. Soc.
- Stump, B. W., L. R. Johnson, 1977. The determination of source properties by the linear inversion of seismograms, Bull. Seism. Soc. Am., 67, 1489-1502.
- Stump, B. W., L. R. Johnson, 1984. Near-field source characteristics of contained nuclear explosions in tuff, Bull. Seism. Soc. Am., 1-26.
- von Seggern, D., R. Blandford, 1972. Source time functions and spectra for underground nuclear explosions, Geophys. J. R. Astr. Soc., 31, 83-97.
- Wallace, T. C., D. V. Helmberger, G. R. Engen, 1983. Evidence of tectonic release from underground nuclear explosions in long-period P waves, Bull. Seism. Soc. Am., 73, 593-613.
- Wallace, T. C., D. V. Helmberger, G. R. Engen, 1985. Evidence of tectonic release from underground nuclear explosions in long-period S waves, Bull. Seism. Soc. Am., 75, 157-174.
- Wallace, T. C., J. S. Barker, 1987. Modeling near-field observations from nuclear explosions in dry tuff and alluvium, Bull. Seism. Soc. Am., in press.

Table 1. Shot Parameters		
	Harzer	Chancellor
Date	6 June 1981	1 Sept 1983
Origin Time	18h 00m 00.1s	14h 00m 00.1s
Latitude	37.303N	37.273N
Longitude	116.326W	116.355W
Surface elevation	2097m	2040m
Depth to shot	637m	625m
Shot Medium	tuff	tuff
Depth to standing water	668m	647m
Magnitude M_L (BRK)	5.4	5.3
Magnitude m_b (USGS)	5.5	5.4

Station	Distance (km)	Azimuth (deg E of N)	Elevation (m)	First Peak Acceleration (cm/sec)			Maximum Acceleration (cm/sec)		
				R	T	V	R	T	V
				H9	2.37	345	2062	113	56
H4	3.47	137	2134	17	6	140	139	140	318
H2	3.52	28	2060	109	-11	115	364	298	410
H1	4.65	5	2112	46	-10	141	137	135	176
H3	4.74	69	2057	8	-2	71	257	144	163
H6	5.61	206	2006	62	6	70	300	324	292
H8	5.78	310	2060	16	-5	37	134	58	75
H5	6.62	167	2112	18	22	46	103	93	105

Station	Distance (km)	Azimuth (deg E of N)	Elevation (m)	First Peak Acceleration (cm/sec)			Maximum Acceleration (cm/sec)		
				R	T	V	R	T	V
				C10	1.84	102	2065	445	34
C3	2.11	241	1981	189	-126	377	788	788	856
C2	2.65	322	1981	48	83	210	598	417	524
C0	3.08	19	2071	130	9	160	341	463	200
C5	4.48	186	2048	70	12	82	270	298	824
C4	5.52	133	2135	49	13	63	118	133	127
C9	5.60	286	1998	45	20	62	140	199	142
C6	6.02	19	2062	28	-2	36	70	84	94
C1	9.34	350	2038	13	5	27	63	121	90
C7	9.81	23	2128	6	-2	6	81	119	56
C8	10.82	260	1885	8	4	43	44	44	60

Table 4. Parameters for Fitting Reduced Displacement Potentials			
		Harzer	Chancellor
Mueller-Murphy			
	$M_{I\infty}$ (10^{20} dyne-cm)	820	600
	Ψ_{∞} (10^{10}cm^3)	3.0	2.2
	τ (sec)	0.55	0.35
	P_1/P_0	3.0	1.5
von Seggern-Blandford			
	$M_{I\infty}$ (10^{20} dyne-cm)	740	570
	Ψ_{∞} (10^{10}cm^3)	2.7	2.1
	τ (sec)	0.50	0.35
	c_2	-2.5	-1.5
Helmberger-Hadley			
	$M_{I\infty}$ (10^{20} dyne-cm)	680	570
	Ψ_{∞} (10^{10}cm^3)	2.5	2.1
	τ (sec)	0.35	0.25
	c_3	-1.0	-0.6
Haskell			
	$M_{I\infty}$ (10^{20} dyne-cm)	730	620
	Ψ_{∞} (10^{10}cm^3)	2.7	2.3
	τ (sec)	0.30	0.20
	c_4	-0.3	-0.15

FIGURE CAPTIONS

- Figure 1. Map showing the locations of the explosions and recording sites in the Pahute Mesa region of the Nevada Test Site. The two explosions Harzer and Chancellor are denoted by open circles and the sites of temporary recording stations are denoted by closed circles.
- Figure 2. Velocities of ground motion for the event Harzer which were obtained by integrating the observed accelerations. The plots have been scaled by multiplying by the epicentral distance (Table 2). The radial direction R is positive away from the source, the transverse direction T is clockwise about the source as viewed from above, and the vertical direction V is positive upward. The seismograms have been shifted to align the first arrivals which corresponds to a reducing velocity of about 4 km/sec.
- Figure 3. Similar to Figure 2 for the event Chancellor.
- Figure 4. Estimates of average material properties for the upper 4 km of the Silent Canyon Caldera.
- Figure 5. Amplitude density spectra of the moment rate tensors estimated for the events Harzer and Chancellor. The solid lines are for the M_{11} elements of the moment tensors, the dashed lines for the M_{33} elements, and the dotted lines for the average deviatoric elements. In the lower parts of the plots are shown the estimated standard errors which were obtained by assuming random white noise in the input data.
- Figure 6. Comparison between the observed and predicted ground velocities for two stations of the event Chancellor. For each component the predicted result is shown directly below the observed data. The amplitude scales are different for each component but are the same for observed and predicted traces. The panel on the left is for station C3 at an epicentral distance of 2.1 km and that on the right is for station C7 at a distance of 9.8 km.
- Figure 7. Time domain estimates of the 6 elements of the second-order moment tensor for the event Harzer.
- Figure 8. Time domain estimates of the 6 elements of the second-order moment tensor for the event Chancellor.
- Figure 9. The spectral amplitude density of the isotropic parts of the moment-rate tensor and the time domain plots of the isotropic parts of the moment tensor for the explosions Harzer and

Chancellor.

- Figure 10. Amplitude and spectral amplitude density (solid lines) of the isotropic part of the estimated moment tensors and the Mueller-Murphy model of the reduced displacement potential (dashed lines) which were fit to the moment tensor results for the events Harzer and Chancellor. The parameters used to achieve these fits are listed in Table 4.
- Figure 11. Amplitude and spectral amplitude density (solid lines) of the isotropic part of the estimated moment tensors and the von Seggern-Blandford model of the reduced displacement potential (dashed lines) which were fit to the moment tensor results for the events Harzer and Chancellor. The parameters used to achieve these fits are listed in Table 4.
- Figure 12. Amplitude and spectral amplitude density (solid lines) of the isotropic part of the estimated moment tensors and the Helmberger-Hadley model of the reduced displacement potential (dashed lines) which were fit to the moment tensor results for the events Harzer and Chancellor. The parameters used to achieve these fits are listed in Table 4.
- Figure 13. Amplitude and spectral amplitude density (solid lines) of the isotropic part of the estimated moment tensors and the Haskell model of the reduced displacement potential (dashed lines) which were fit to the moment tensor results for the events Harzer and Chancellor. The parameters used to achieve these fits are listed in Table 4.
- Figure 14. Eigenvalues of the deviatoric elements of the estimated moment tensors for the events Harzer and Chancellor.
- Figure 15. Lower-hemisphere equal-area stereographic plot of the directions of the eigenvectors of the estimated deviatoric moment tensor for the events Harzer and Chancellor. The directions are shown for the time interval 0.5-3 sec. Also plotted as triangles are the positions of the recording sites as they are projected onto the focal sphere along the path of the direct P wave.
- Figure 16. Observed and predicted seismograms at station C10 at a distance of 1.8 km from the explosion Chancellor.

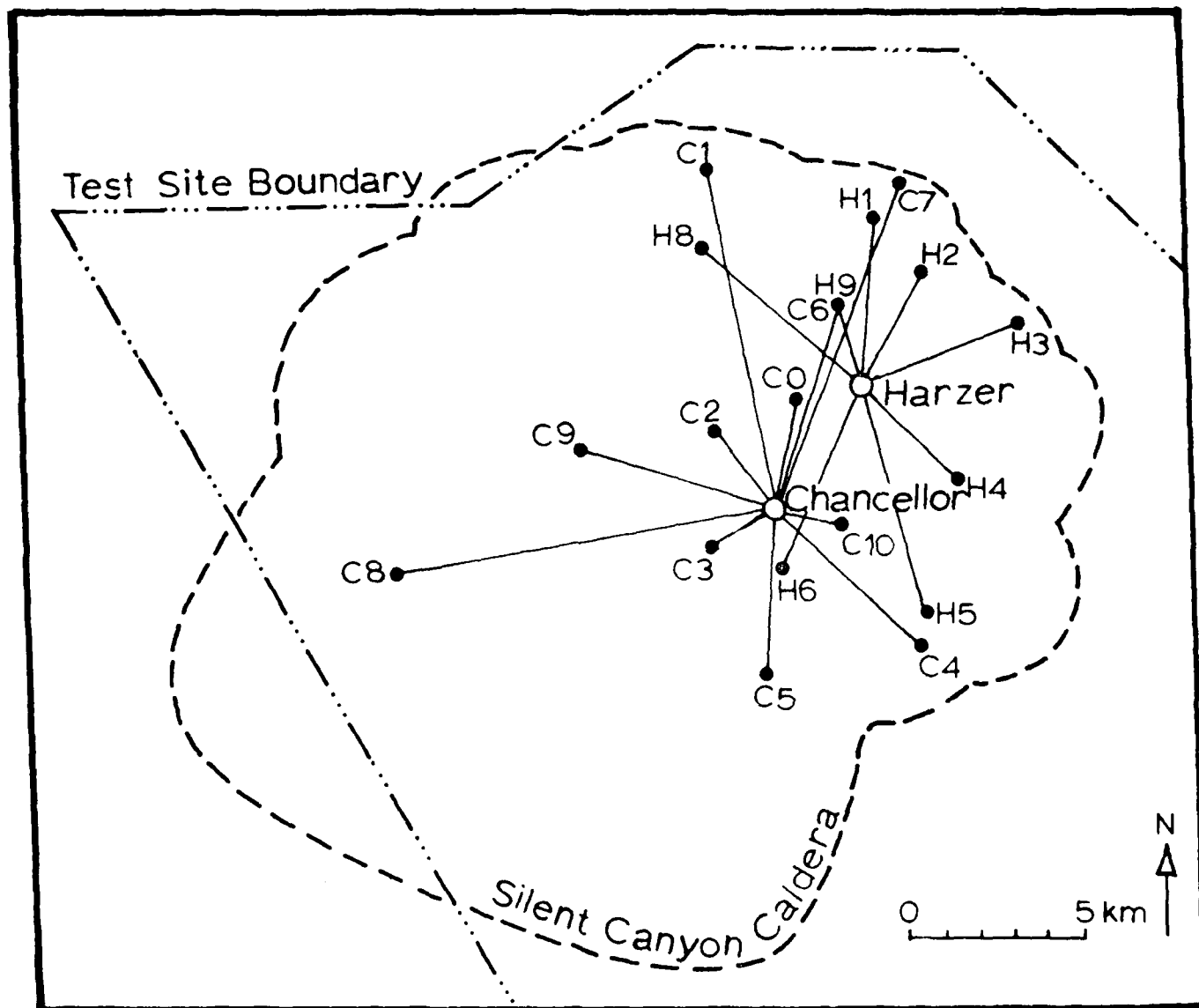


Figure 1

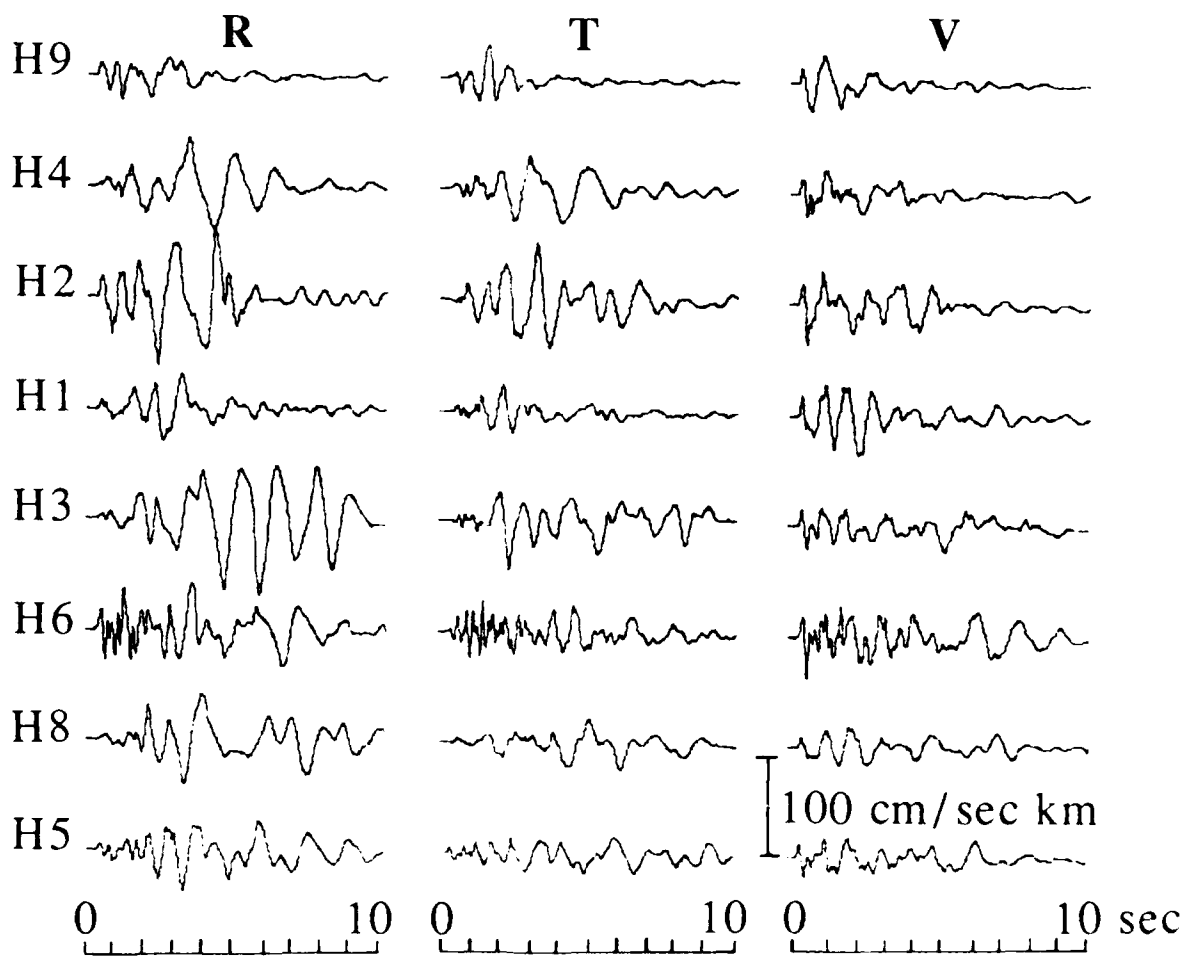


Figure 2

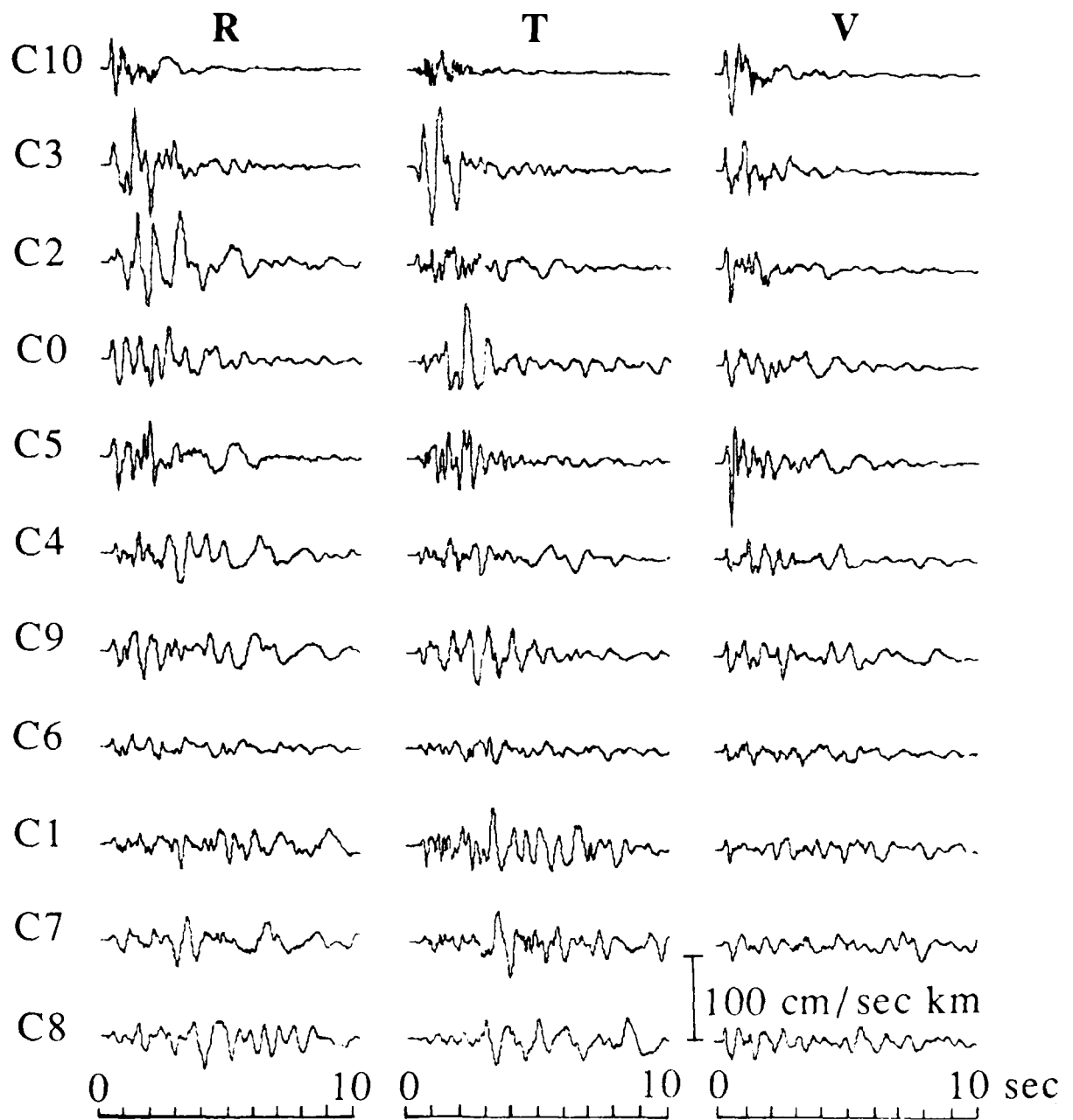
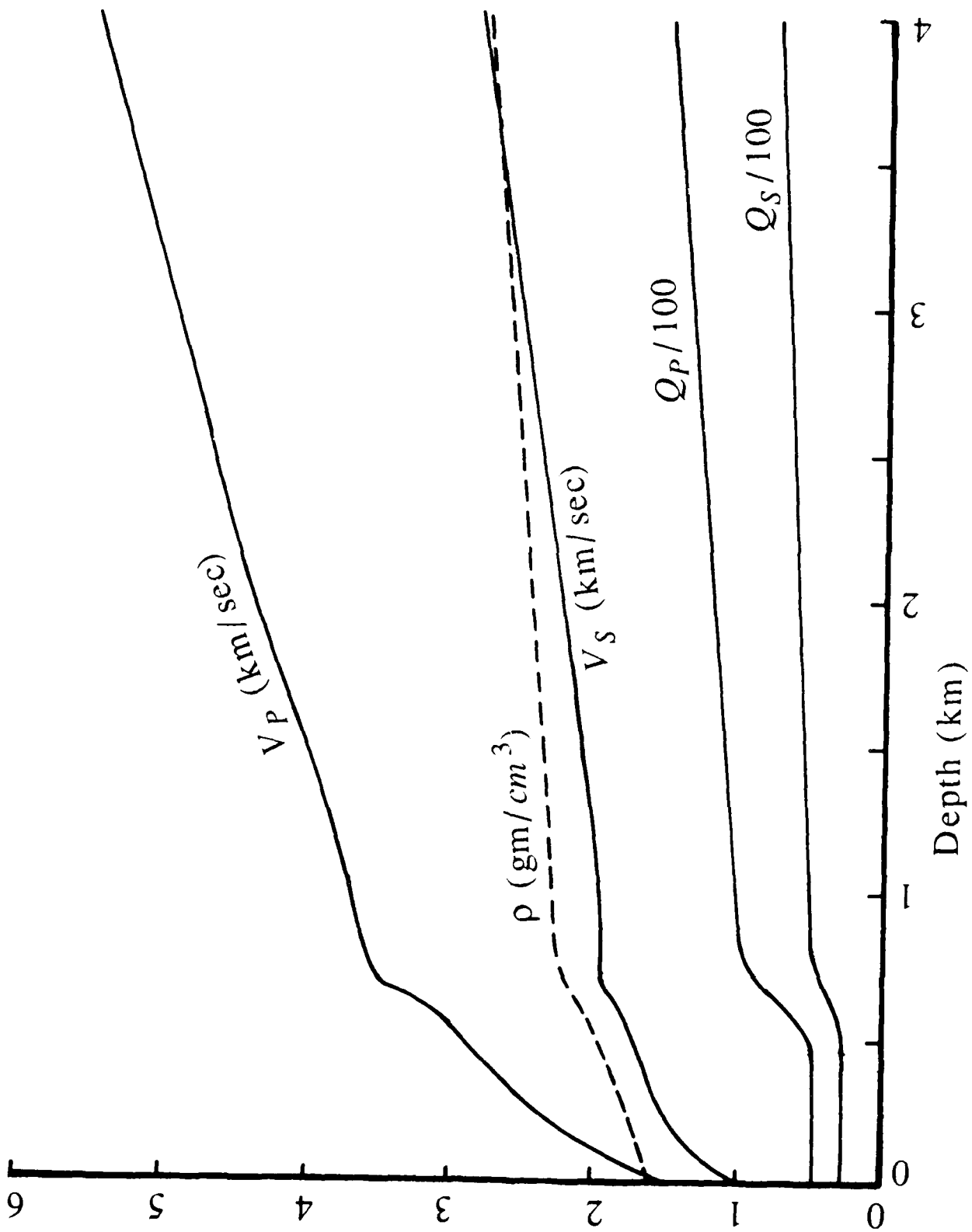


Figure 3



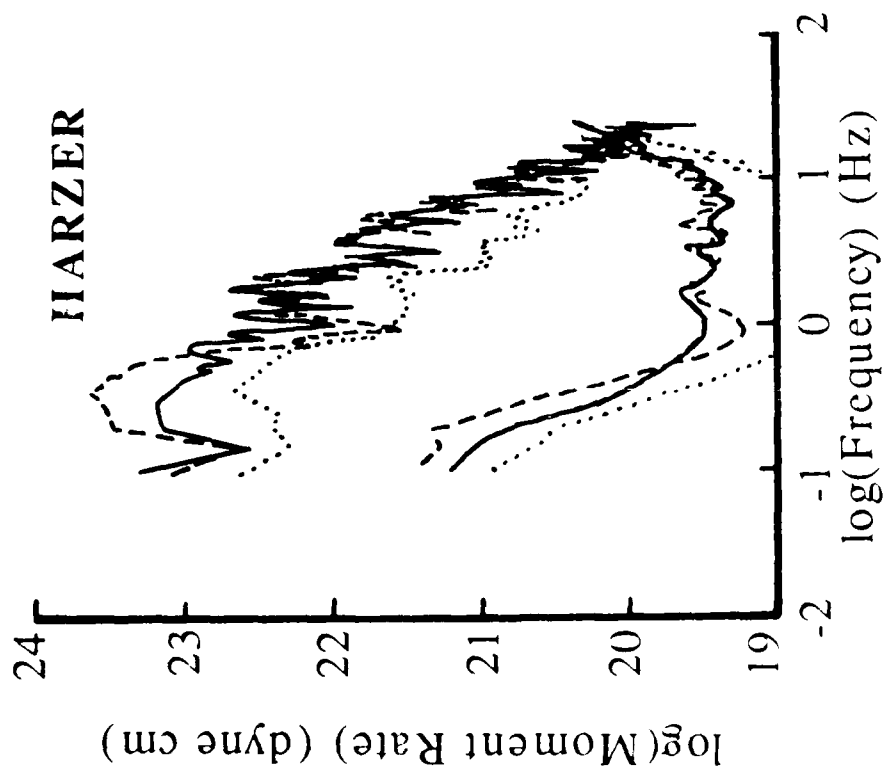
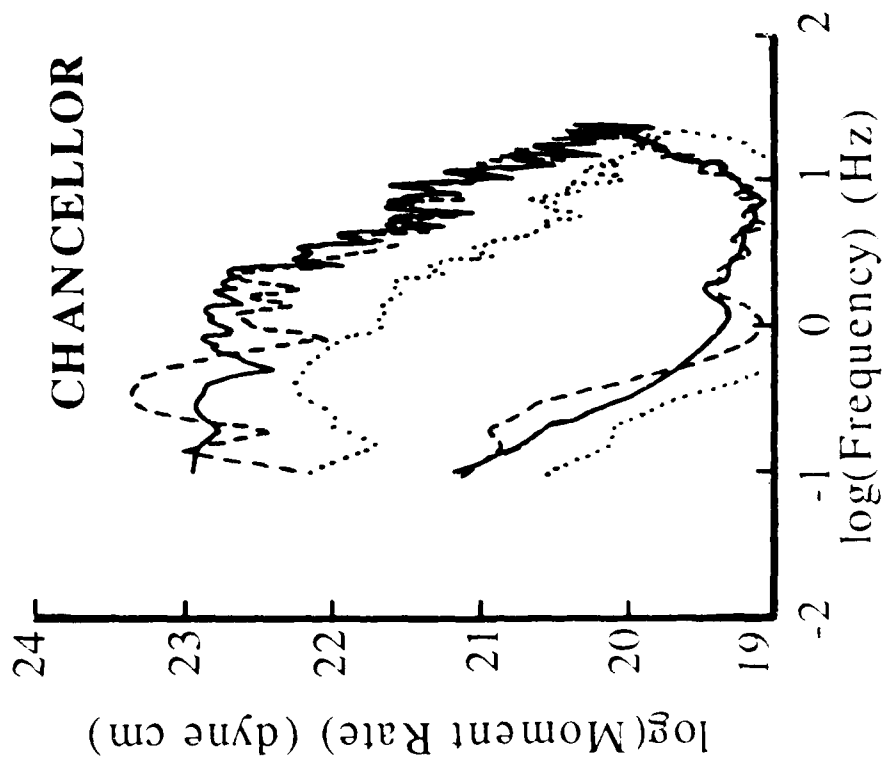


Figure 5

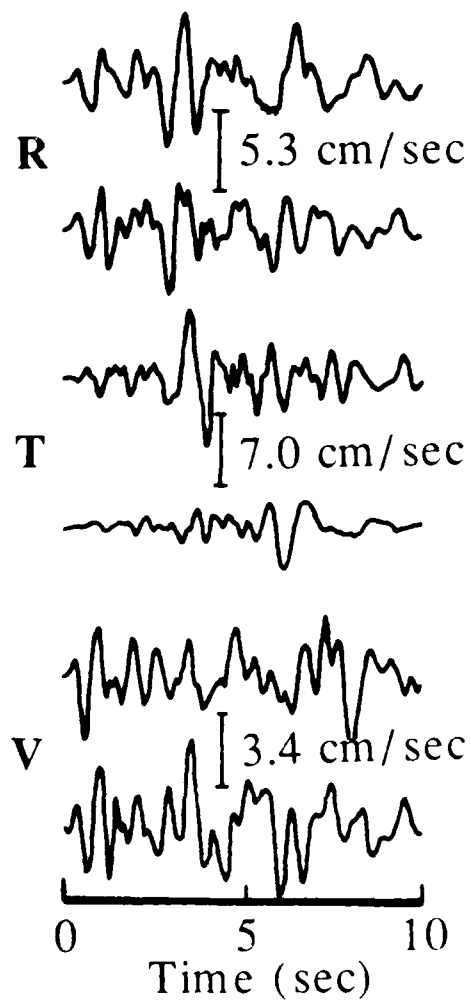
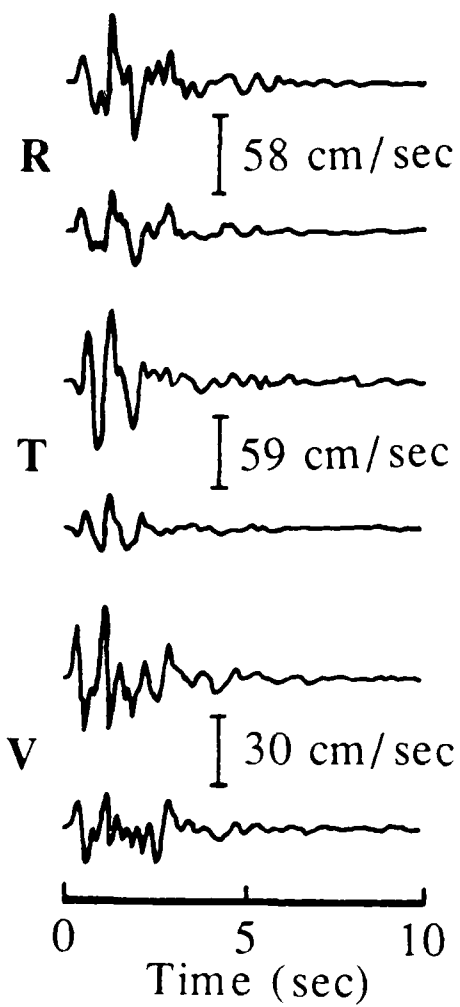
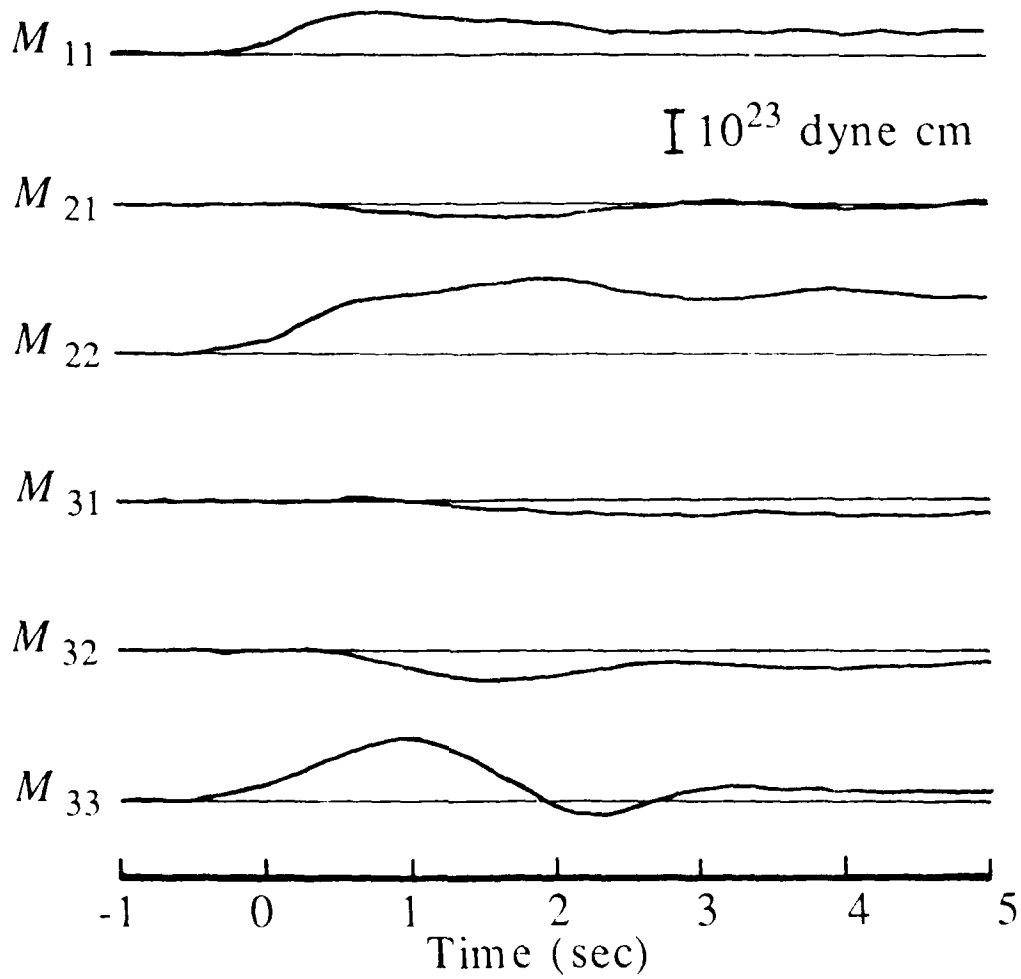


Figure 6

HARZER



CHANCELLOR

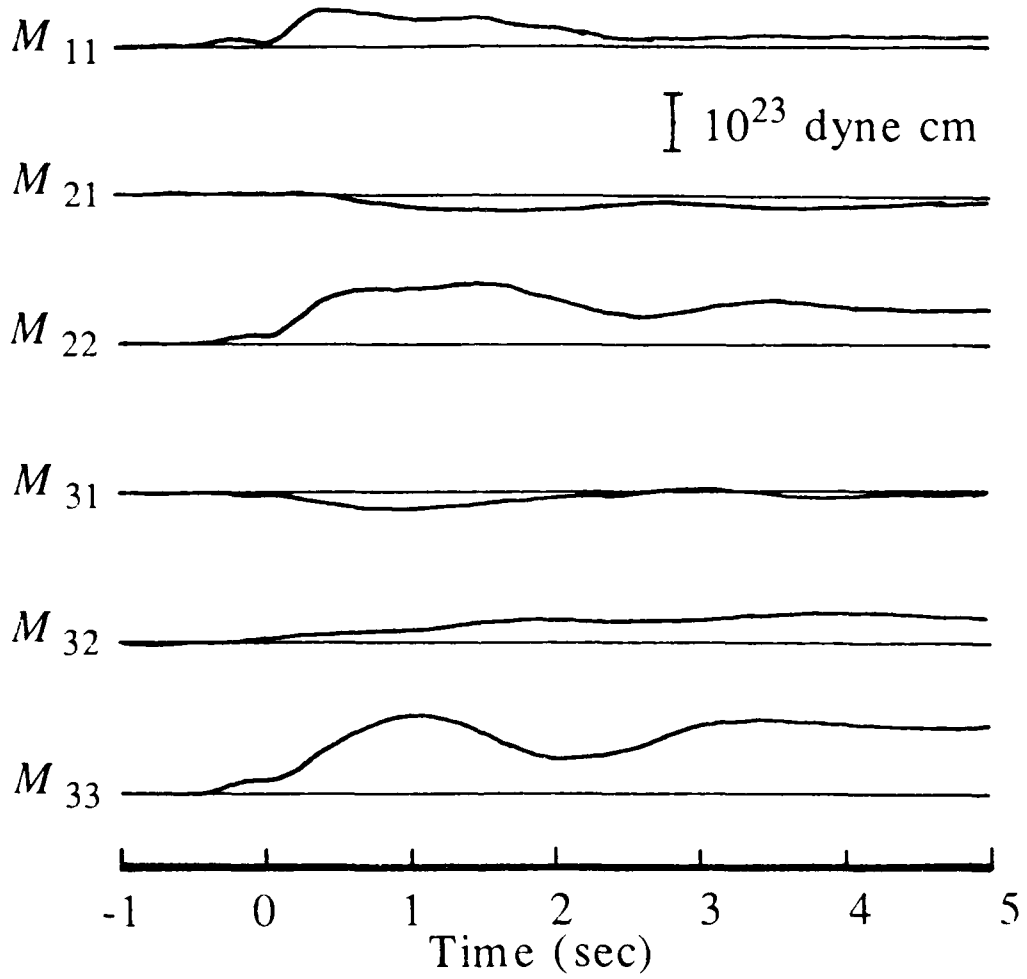


Figure 8

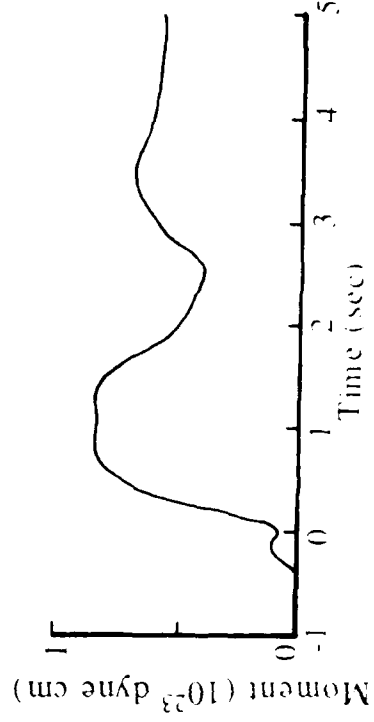
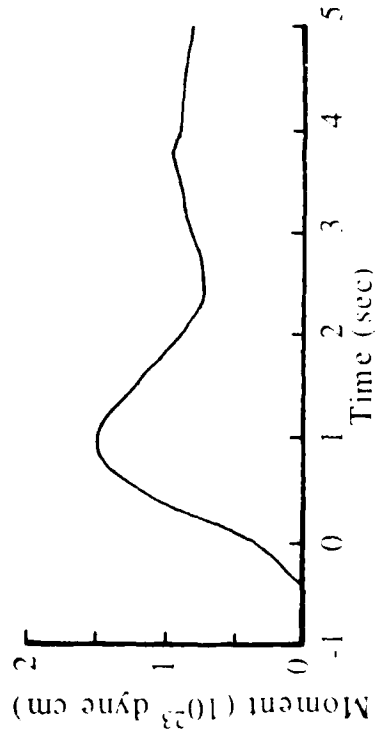
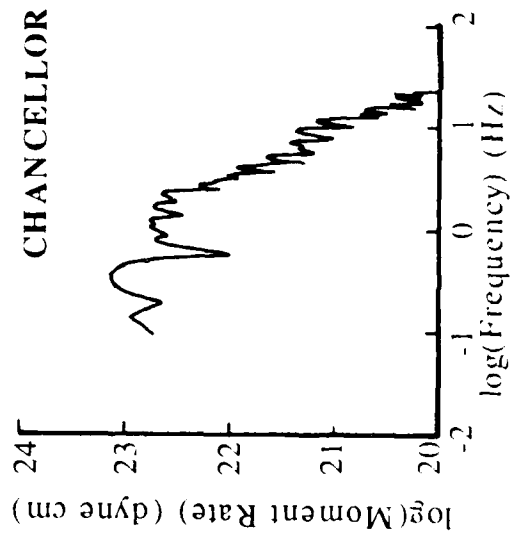
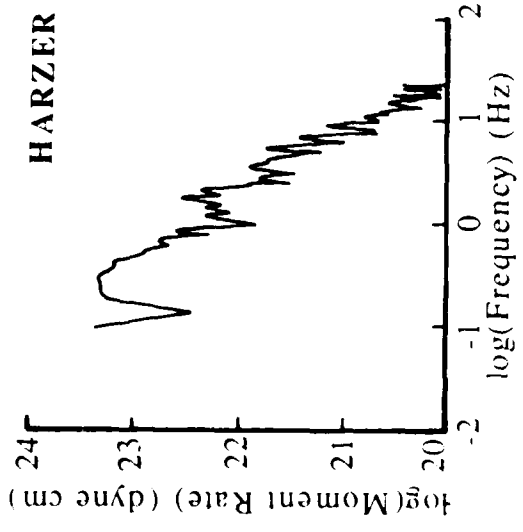


Figure 9

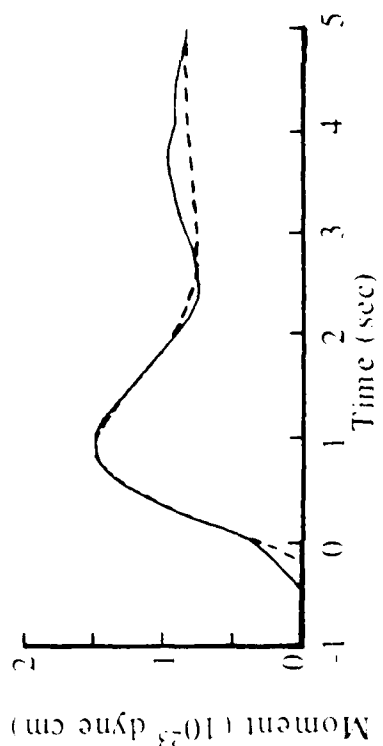
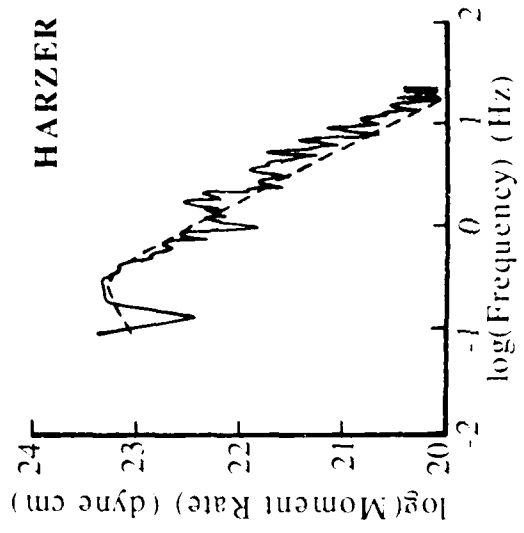
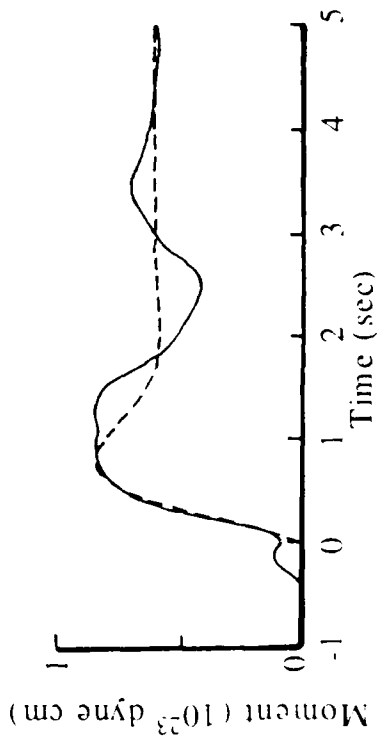
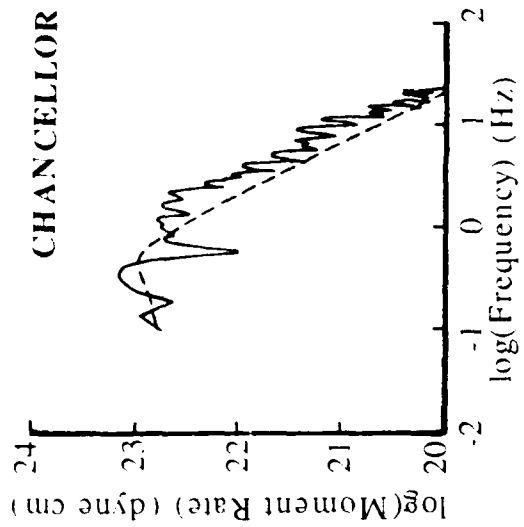


Figure 10

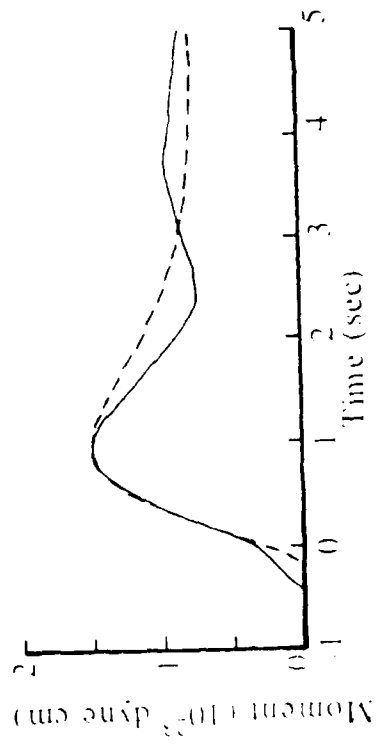
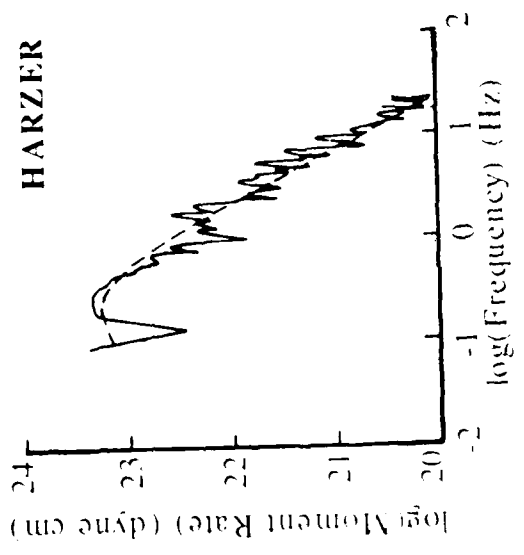
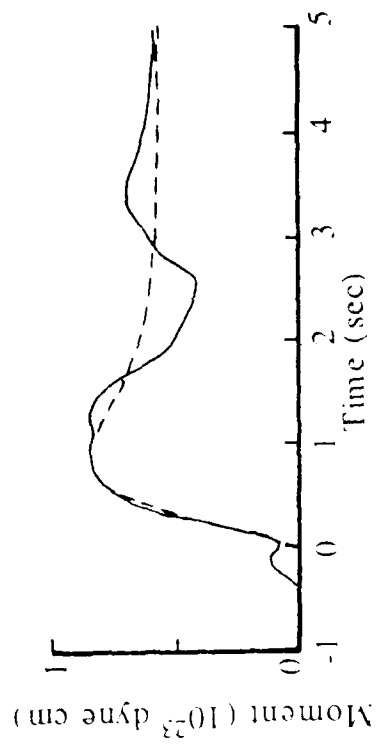
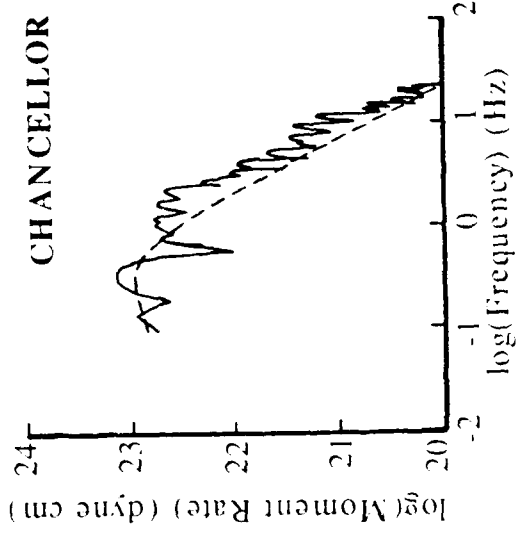


Figure 11

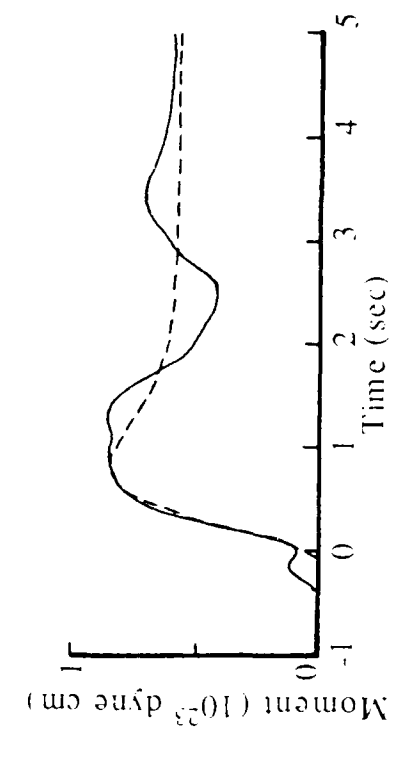
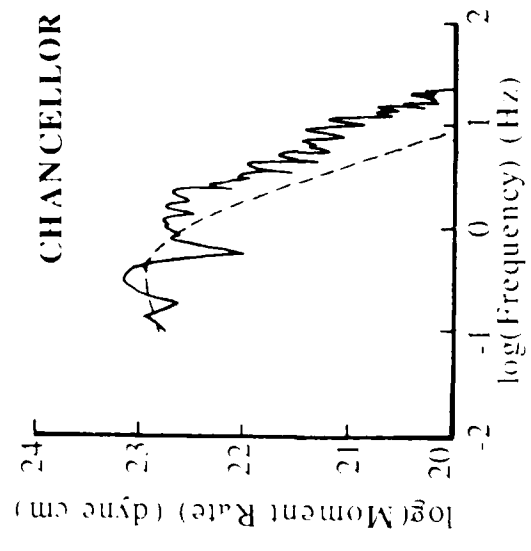
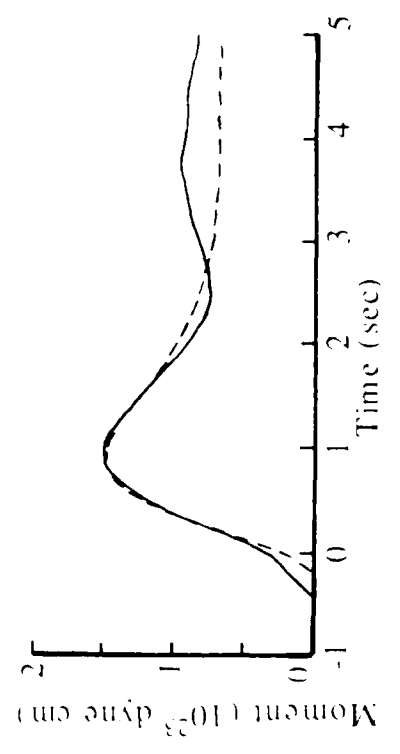
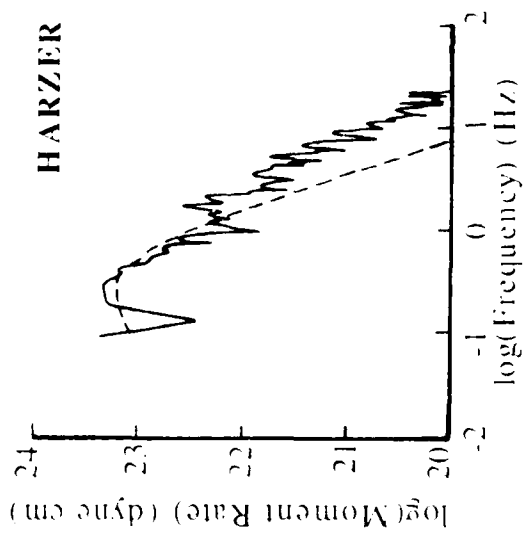


Figure 12

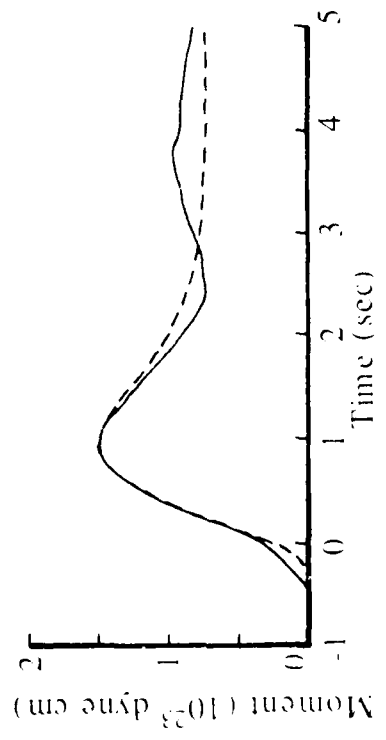
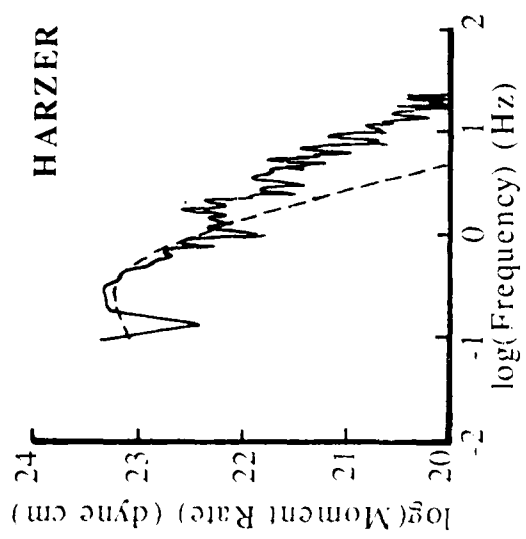
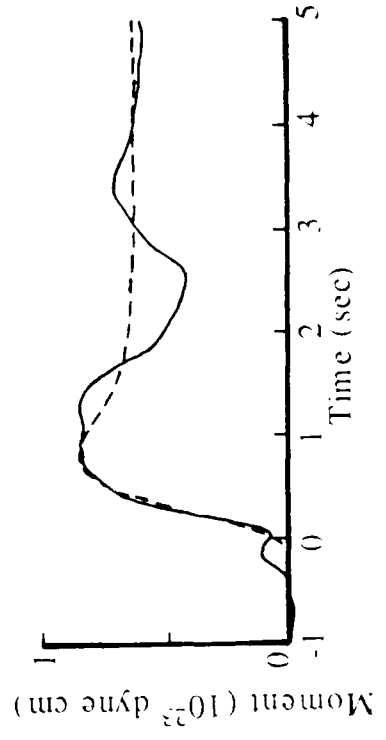
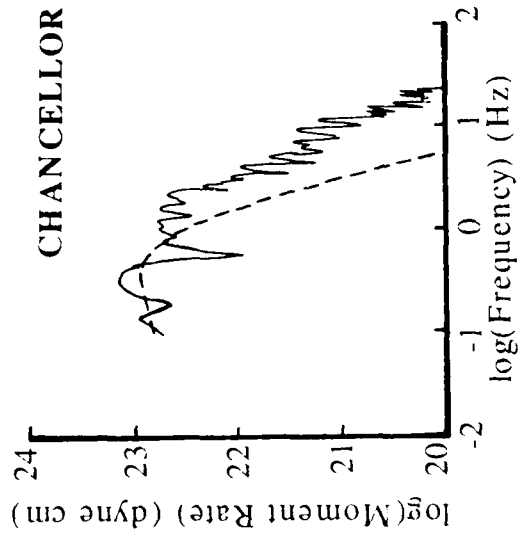


Figure 13

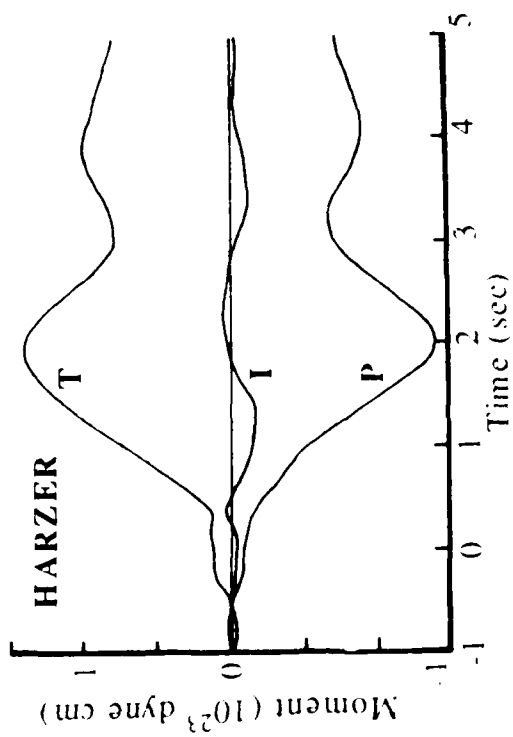
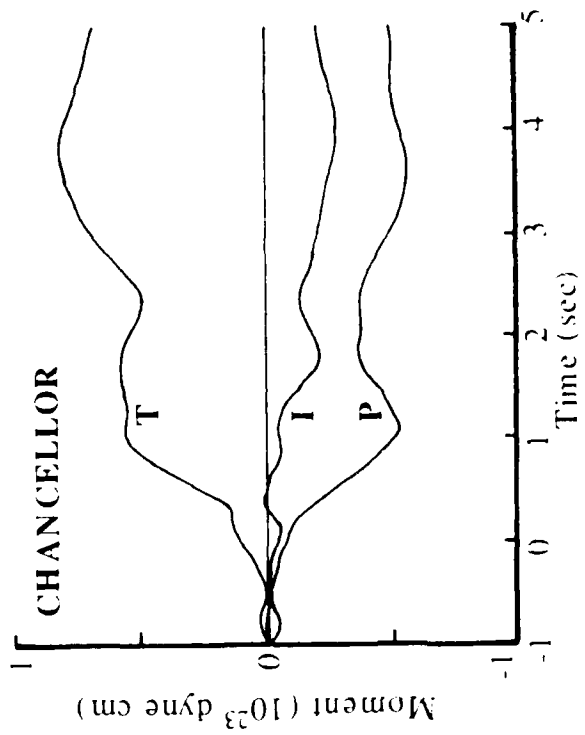


Figure 14

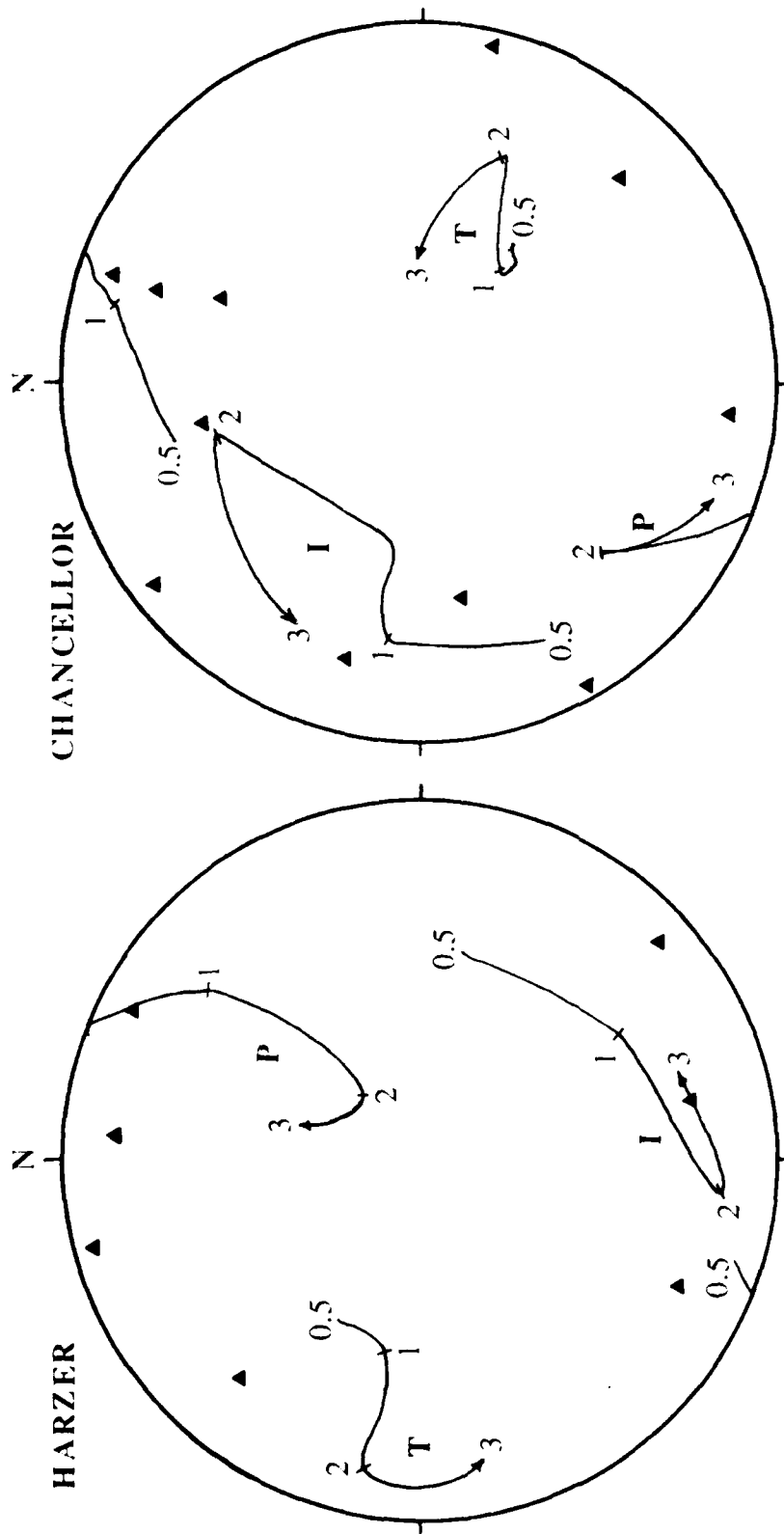


Figure 15

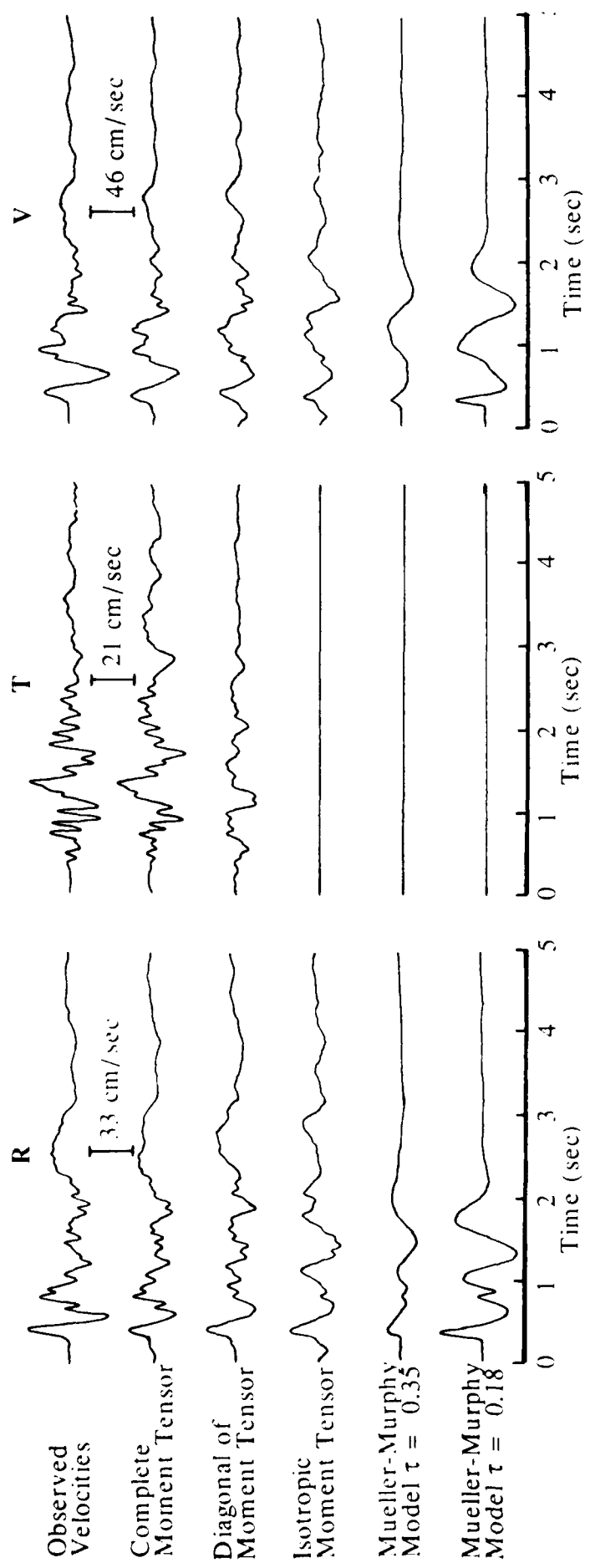


Figure 16

Professor Keiiti Aki
Center for Earth Sciences
University of Southern California
University Park
Los Angeles, CA 90089-0741

Cooperative Institute for Resch
in Environmental Sciences
University of Colorado
Boulder, CO 80309

Dr. Thomas C. Bache Jr.
Science Applications Int'l Corp.
10210 Campus Point Drive
San Diego, CA 92121 (2 copies)

Dr. Douglas R. Baumgardt
Signal Analysis & Systems Div.
ENS CO, Inc.
5400 Port Royal Road
Springfield, VA 22151-2388

Dr. S. Bratt
Science Applications Int'l Corp.
10210 Campus Point Drive
San Diego, CA 92121

Dr. Lawrence J. Burdick
Woodward-Clyde Consultants
P.O. Box 93245
Pasadena, CA 91109-3245 (2 copies)

Professor Robert W. Clayton
Seismological Laboratory/Div. of
Geological & Planetary Sciences
California Institute of Technology
Pasadena, CA 91125

Dr. Vernon F. Cormier
Department of Geology & Geophysics
U-45, Room 207
The University of Connecticut
Storrs, Connecticut 06268

Dr. Zoltan A. Der
ENS CO, Inc.
5400 Port Royal Road
Springfield, VA 22151-2388

Professor John Ferguson
Center for Lithospheric Studies
The University of Texas at Dallas
P.O. Box 830688
Richardson, TX 75083-0688

OCT87

Professor Stanley Flatte'
Applied Sciences Building
University of California, Santa Cruz
Santa Cruz, CA 95064

Professor Steven Grand
Department of Geology
245 Natural History Building
1000 University Drive
Berkeley, CA 94720

Professor Roy Greenfield
Geosciences Department
403 Deike Building
The Pennsylvania State University
University Park, PA 16802

Professor David G. Harkrider
Seismological Laboratory
Div of Geological & Planetary Sciences
California Institute of Technology
Pasadena, CA 91125

Professor Donald V. Helmberger
Seismological Laboratory
Div of Geological & Planetary Sciences
California Institute of Technology
Pasadena, CA 91125

Professor Eugene Herrin
Institute for the Study of Earth
& Man/Geophysical Laboratory
Southern Methodist University
Dallas, TX 75275

Professor Robert B. Herrmann
Department of Earth & Atmospheric
Sciences
Saint Louis University
Saint Louis, MO 63156

Professor Lane R. Johnson
Seismographic Station
University of California
Berkeley, CA 94720

Professor Thomas H. Jordan
Department of Earth, Atmospheric
and Planetary Sciences
Mass Institute of Technology
Cambridge, MA 02139

Dr. Alan Kafka
Department of Geology &
Geophysics
Boston College
Chestnut Hill, MA 02167

Professor Leon Knopoff
University of California
Institute of Geophysics
& Planetary Physics
Los Angeles, CA 90024

Professor Charles A. Langston
Geophysics Department

The Pennsylvania State University
University Park, PA 16802

Professor Thorne Lay
Department of Geological Sciences
1006 C.C. Little Building
University of Michigan
Ann Harbor, MI 48109-1063

Dr. Randolph Martin III
New England Research, Inc.
P.O. Box 857
Norwich, VT 05055

Dr. Gary McCartor
Mission Research Corp.
735 State Street
P.O. Drawer 719
Santa Barbara, CA 93102 (2 copies)

Professor Thomas V. McEvelly
Seismographic Station
University of California
Berkeley, CA 94720

Dr. Keith L. McLaughlin
Teledyne Geotech
314 Montgomery Street
Alexandria, VA 22314

Professor William Menke
Lamont-Doherty Geological Observatory
of Columbia University
Palisades, NY 10964

Professor Brian J. Mitchell
Department of Earth & Atmospheric
Sciences
Saint Louis University
Saint Louis, MO 63156

Mr. Jack Murphy
S-CUBED
A Division of Maxwell Laboratory
11800 Sunrise Valley Drive
Suite 1212
Reston, VA 22091 (2 copies)

Professor Otto W. Nuttli
Department of Earth &
Atmospheric Sciences
Saint Louis University
Saint Louis, MO 63156

Professor J. A. Orcutt
Institute of Geophysics and Planetary

Scripps Institute of Oceanography
Univ. of California, San Diego
La Jolla, CA 92093

Professor Keith Priestley
University of Nevada
Mackay School of Mines
Reno, Nevada 89557

Professor Charles G. Sammis
Center for Earth Sciences
University of Southern California
University Park
Los Angeles, CA 90089-0741

Dr. Jeffrey L. Stevens
S-CJBED,
A Division of Maxwell Laboratory
P.O. Box 1620
La Jolla, CA 92038-1620

Professor Brian Stump
Institute for the Study of Earth & Man
Geophysical Laboratory
Southern Methodist University
Dallas, TX 75275

Professor Ta-liang Teng
Center for Earth Sciences
University of Southern California
University Park
Los Angeles, CA 90089-0741

Professor M. Nafi Toksoz
Earth Resources Lab
Dept of Earth, Atmospheric and
Planetary Sciences
Massachusetts Institute of Technology
42 Carleton Street
Cambridge, MA 02142

Professor Terry C. Wallace
Department of Geosciences
Building #11
University of Arizona
Tucson, AZ 85721

Professor Francis T. Wu
Department of Geological Sciences
State University of new York
At Binghamton
Vestal, NY 13901

OCT87

Dr. Monem Abdel-Gawad
Rockwell Internat'l Science Center
1049 Camino Dos Rios
Thousand Oaks, CA 91360

Professor Shelton S. Alexander

403 Leike Building
The Pennsylvania State University
University Park, PA 16802

Dr. Muawia Barazangi
Geological Sciences
Cornell University
Ithaca, NY 14853

Mr. William J. Best
907 Westwood Drive
Vienna, VA 22180

Dr. N. Biswas
Geophysical Institute
University of Alaska
Fairbanks, AK 99701

Dr. G. A. Bollinger
Department of Geological Sciences
Virginia Polytechnical Institute
21044 Derring Hall
Blacksburg, VA 24061

Dr. James Bulau
Rockwell Int'l Science Center
1049 Camino Dos Rios
P.O. Box 1085
Thousand Oaks, CA 91360

Mr. Roy Burger
1221 Serry Rd.
Schenectady, NY 12309

Dr. Robert Burrige
Schlumberger-Doll Resch Cr.
Old Quarry Road
Ridgefield, CT 06877

Professor Jon F. Claerbout
Professor Amos Nur
Dept. of Geophysics
Stanford University
Stanford, CA 94305 (2 copies)

Dr. Anton W. Dainty
AFGL/LWH
Hanscom AFB, MA 01731

Professor Adam Dziewonski
Hoffman Laboratory
Harvard University
20 Oxford St.
Cambridge, MA 02138

OCT87

Professor John Ebel
Dept of Geology & Geophysics

Chestnut Hill, MA 02167

Dr. Alexander Florence
SRI International
333 Ravenwood Avenue
Menlo Park, CA 94025-3493

Dr. Donald Forsyth
Dept. of Geological Sciences
Brown University
Providence, RI 02912

Dr. Anthony Gangi
Texas A&M University
Department of Geophysics
College Station, TX 77843

Dr. Freeman Gilbert
Institute of Geophysics &
Planetary Physics
Univ. of California, San Diego
P.O. Box 109
La Jolla, CA 92037

Mr. Edward Giller
Pacific Seirra Research Corp.
1401 Wilson Boulevard
Arlington, VA 22209

Dr. Jeffrey W. Given
Sierra Geophysics
11255 Kirkland Way
Kirkland, WA 98033

Dr. Arthur Lerner-Lam
Lamont-Doherty Geological Observatory
of Columbia University
Palisades, NY 10964

Dr. L. Timothy Long
School of Geophysical Sciences
Georgia Institute of Technology
Atlanta, GA 30332

Dr. George R. Mellman
Sierra Geophysics
11255 Kirkland Way
Kirkland, WA 98033

Science Horizons, Inc.
ATTN: Dr. Bernard Minster
Dr. Theodore Cherry
710 Encinitas Blvd., Suite 101
Encinitas, CA 92024 (2 copies)

Dr. Geza Nagy
Menlo Park, CA 94025-3493

Dr. Jack Oliver
Department of Geology
Cornell University
Ithaca, NY 14850

Dr. Robert Phinney/Dr. F.A. Dahlen
Dept of Geological
Geophysical Sci. University
Princeton University
Princeton, NJ 08540 (2 copies)

Professor Paul G. Richards
Lamont-Doherty Geological
Observatory of Columbia Univ.
Palisades, NY 10964

Dr. Norton Rimer
S-CUBED
A Division of Maxwell Laboratory
P.O. 1620
La Jolla, CA 92038-1620

Professor Larry J. Ruff
Department of Geological Sciences
1006 C.C. Little Building
University of Michigan
Ann Arbor, MI 48109-1063

Dr. Alan S. Ryall, Jr.
Center of Seismic Studies
1300 North 17th Street
Suite 1450
Arlington, VA 22209-2308 (4 copies)

Dr. David G. Simpson
Lamont-Doherty Geological Observ.
of Columbia University
Palisades, NY 10964

Dr. Bob Smith
Department of Geophysics
University of Utah
1400 East 2nd South
Salt Lake City, UT 84112

Dr. S. W. Smith
Geophysics Program
University of Washington
Seattle, WA 98195

Rondout Associates
ATTN: Dr. George Sutton,
Dr. Jerry Carter, Dr. Paul Pomeroy

Stone Ridge, NY 12484 (4 copies)

Dr. L. Sykes
Lamont Doherty Geological Observ.
Columbia University
Palisades, NY 10964

Dr. Pradeep Talwani
Department of Geological Sciences
University of South Carolina
Columbia, SC 29208

Dr. R. B. Tittmann
Rockwell International Science Center
1049 Camino Dos Rios
P.O. Box 1085
Thousand Oaks, CA 91360

Weidlinger Associates
ATTN: Dr. Gregory Wojcik
620 Hansen Way, Suite 100
Palo Alto, CA 94304

Professor John H. Woodhouse
Hoffman Laboratory
Harvard University
20 Oxford St.
Cambridge, MA 02138

Dr. Gregory B. Young
ENSCO, Inc.
5400 Port Royal Road
Springfield, VA 22151-2388

Peter Basham
Earth Physics Branch
Geological Survey of Canada
1 Observatory Crescent
Ottawa, Ontario
CANADA K1A 0Y3

Dr. Eduard Berg
Institute of Geophysics
University of Hawaii
Honolulu, HI 96822

Dr. Michel Bouchon - Universite
Scientifique et Medicale de Grenoble
Lab de Geophysique - Interne et
Tectonophysique - I.R.I.G.M.-B.P.
38402 St. Martin D'Herès
Cedex FRANCE

Dr. Hilmar Bungum/NTNF/NORSAR
P.O. Box 51
Norwegian Council of Science,
Industry and Research, NORSAR
N-2007 Kjeller, NORWAY

Dr. Michel Campillo
I.R.I.G.M.-B.P. 68
38402 St. Martin D'Herès
Cedex, FRANCE

Dr. Kin-Yip Chun
Geophysics Division
Physics Department
University of Toronto
Ontario, CANADA M5S 1A7

Dr. Alan Douglas
Ministry of Defense
Blacknest, Brimpton,
Reading RG7-4RS
UNITED KINGDOM

Dr. Manfred Henger
Fed. Inst. for Geosciences & Nat'l Res.
Postfach 510153
D-3000 Hannover 51
FEDERAL REPUBLIC OF GERMANY

Dr. E. Husebye
NTNF/NORSAR
P.O. Box 51
N-2007 Kjeller, NORWAY

OCT87

Mr. Peter Marshall, Procurement
Executive, Ministry of Defense
Blacknest, Brimpton,
Reading RG7-4RS
UNITED KINGDOM (3 copies)

Dr. Ben Menaheim
Weizman Institute of Science

Dr. Svein Mykkeltveit
NTNF/NORSAR
P.O. Box 51
N-2007 Kjeller, NORWAY (3 copies)

Dr. Robert North
Geophysics Division
Geological Survey of Canada
1 Observatory crescent
Ottawa, Ontario
CANADA, K1A 0Y3

Dr. Frode Ringdal
NTNF/NORSAR
P.O. Box 51
N-2007 Kjeller, NORWAY

Dr. Jorg Schlittenhardt
Federal Inst. for Geosciences & Nat'l Res.
Postfach 510153
D-3000 Hannover 51
FEDERAL REPUBLIC OF GERMANY

University of Hawaii
Institute of Geophysics
ATTN: Dr. Daniel Walker
Honolulu, HI 96822

Dr. Ramon Cabre, S.J.
c/o Mr. Ralph Buck
Economic Consular
American Embassy
APO Miami, Florida 34032

Institute for Geophysik
Rhur University/Bochum
P.O. Box 102148, 4630 Bochum 1
FEDERAL REPUBLIC OF GERMANY

Professor Brian L.N. Kennett
Research School of Earth Sciences
Institute of Advanced Studies
G.P.O. Box 4
Canberra 2601
AUSTRALIA

Dr. B. Massinon
Societe Radiomana
27, Rue Claude Bernard
7,005, Paris, FRANCE (2 copies)

Dr. Pierre Mechler
Societe Radiomana
27, Rue Claude Bernard
75005, Paris, FRANCE

Dr. Ralph Alewine III
DARPA/NMRO
1400 Wilson Boulevard
Arlington, VA 22209-2308

Dr. Robert Blandford

1400 Wilson Boulevard
Arlington, VA 22209-2308

Sandia National Laboratory
ATTN: Dr. H. B. Durham
Albuquerque, NM 87185

Dr. Jack Evernden
USGS-Earthquake Studies
345 Middlefield Road
Menlo Park, CA 94025

U.S. Geological Survey
ATTN: Dr. T. Hanks
Nat'l Earthquake Resch Center
345 Middlefield Road
Menlo Park, CA 94025

Dr. James Hannon
Lawrence Livermore Nat'l Lab.
P.O. Box 808
Livermore, CA 94550

U.S. Arms Control & Disarm. Agency
ATTN: Mrs. M. Hoinkes
Div. of Multilateral Affairs
Room 5499
Washington, D.C. 20451

Paul Johnson
ESS-4, Mail Stop J979
Los Alamos National Laboratory
Los Alamos, NM 87545

Ms. Ann Kerr
DARPA/NMRO
1400 Wilson Boulevard
Arlington, VA 22209-2308

Dr. Max Koontz
US Dept of Energy/DP 331
Forrestal Building
1000 Independence Ave.
Washington, D.C. 20585

Dr. W. H. K. Lee
USGS
Office of Earthquakes, Volcanoes,
& Engineering
Branch of Seismology
345 Middlefield Rd
Menlo Park, CA 94025

OCT87

USGS
Mail Stop 928
Reston, VA 22092

Dr. Robert Masse'
Box 25046, Mail Stop 967
Denver Federal Center
Denver, Colorado 80225

Dr. Keith K. Nakanishi
Lawrence Livermore National Laboratory
P.O. Box 808, L-205
Livermore, CA 94550 (2 copies)

Dr. Carl Newton
Los Alamos National Lab.
P.O. Box 1663
Mail Stop C335, Group E553
Los Alamos, NM 87545

Dr. Kenneth H. Olsen
Los Alamos Scientific Lab.
Post Office Box 1663
Los Alamos, NM 87545

Howard J. Patton
Lawrence Livermore National Laboratory
P.O. Box 808, L-205
Livermore, CA 94550

HQ AFTAC/TG
Attn: Dr. Frank F. Pilotte
Patrick AFB, Florida 32925-6001

Mr. Jack Rachlin
USGS - Geology, Rm 3 C136
Mail Stop 928 National Center
Reston, VA 22092

Robert Reinke
AFWL/NTESG
Kirtland AFB, NM 87117-6008

HQ AFTAC/TGR
Attn: Dr. George H. Rothe
Patrick AFB, Florida 32925-6001

Donald L. Springer
Lawrence Livermore National Laboratory
P.O. Box 808, L-205
Livermore, CA 94550

Dr. Lawrence Turnbull
OSWR/NED
Central Intelligence Agency

Washington, D.C. 20505

Dr. Thomas Weaver
Los Alamos Scientific Laboratory
Los Alamos, NM 97544

AFGL/SULL
Research Library
Hanscom AFB, MA 01731-5000 (2 copies)

Secretary of the Air Force (SAFRD)
Washington, DC 20330
Office of the Secretary Defense
DDR & E
Washington, DC 20330

HQ DNA
ATTN: Technical Library
Washington, DC 20305

Director, Technical Information
DARPA
1400 Wilson Blvd.
Arlington, VA 22209

AFGL/XO
Hanscom AFB, MA 01731-5000

AFGL/LW
Hanscom AFB, MA 01731-5000

DARPA/PM
1400 Wilson Boulevard
Arlington, VA 22209

Defense Technical
Information Center
Cameron Station
Alexandria, VA 22314
(12 copies)

Defense Intelligence Agency
Directorate for Scientific &
Technical Intelligence
Washington, D.C. 20301

OCT87

Defense Nuclear Agency/SPSS
ATTN: Dr. Michael Shore
6801 Telegraph Road
Alexandria, VA 22310

AFOSR/NPG
ATTN: Director

Bolling AFB, Wash D.C. 20332

AFTAC/CA (STINFO)
Patrick AFB, FL 32925-6001

END

DATE

FILMED

5-88

DTIC